General Disclaimer

One or more of the Following Statements may affect this Document

- This document has been reproduced from the best copy furnished by the organizational source. It is being released in the interest of making available as much information as possible.

- This document may contain data, which exceeds the sheet parameters. It was furnished in this condition by the organizational source and is the best copy available.

- This document may contain tone-on-tone or color graphs, charts and/or pictures, which have been reproduced in black and white.

- This document is paginated as submitted by the original source.

- Portions of this document are not fully legible due to the historical nature of some of the material. However, it is the best reproduction available from the original submission.

Produced by the NASA Center for Aerospace Information (CASI)

ANALYSIS OF GRAVITY ASSISTED TRAJECTORIES FOR SOLAR-PROBE AND DEEP-SPACE MISSIONS

NOV 1969
RECEIVED
NASA STI FACILITY
INPUT BRANCH

By

John W. Young

Thesis submitted to the Graduate Faculty of the

Virginia Polytechnic Institute

in partial fulfillment for the degree of

MASTER OF SCIENCE

in

Physics

FACILITY FORM 602

N69-41186
(ACCESSION NUMBER)
92
(NASA CR OR TMX OR AD NUMBER)
TMX-61970
(THRU)
1
(CODE)
30
(CATEGORY)

May 1969

ANALYSIS OF GRAVITY ASSISTED TRAJECTORIES FOR SOLAR-PROBE AND DEEP-SPACE MISSIONS

by

John W. Young

Thesis submitted to the Graduate Faculty of the

Virginia Polytechnic Institute

in partial fulfillment for the degree of

MASTER OF SCIENCE

in

Physics

APPROVED:

Chairman, Dr. A. Keith Furr

Dr. James A. Jacobs

Dr. R. F. Tipsword

Dr. R. J. Adler

May 1969

Blacksburg, Virginia

TABLE OF CONTENTS

CHAPTER	PAGE
TITLE	i
TABLE OF CONTENTS	ii
LIST OF TABLES AND FIGURES	iv
INTRODUCTION	1
NOTATION	5
SURVEY OF LITERATURE	8
THEORY	11
Assumptions	12
Pre-Encounter Transfer Orbit from Earth	13
Initial Conditions at Earth	13
Orbital Parameters for Pre-Encounter Transfer	14
Hyperbolic Encounter at Planet	16
Approach Conditions at Planet Activity Sphere	16
Hyperbolic Orbit at Perturbing Planet	18
Departure Conditions at Planet Activity Sphere	18
Post-Encounter Transfer Orbit	20
Transfer Times and Angles	20
Heliocentric Transfer from Earth to Planet Inside Earth Orbit	20
Heliocentric Transfer from Earth to Planet Outside Earth Orbit	21
Post-Encounter Transfer Orbit	21
Necessary Conditions at Insertion and Encounter	22
Insertion Conditions	22

CHAPTER PAGE

Encounter Conditions 23

RESULTS AND DISCUSSION 24

Direct Transfer Orbits from Earth 24

Solar Probe Missions 25

Venus Flyby 25

Jupiter Flyby 29

Deep-Space Missions 33

Venus Flyby 33

Jupiter Flyby 33

Guidance Analysis for Flyby Missions 34

Approach Corridor Analysis 35

Venus Encounter Corridors 36

Jupiter Encounter Corridors 37

SUMMARY AND CONCLUSIONS 41

REFERENCES 43

APPENDIX A 44

Summary of Equations Used in Analysis of Planetary Flyby. . 44

APPENDIX B 53

Description of Optimization Procedure 53

ACKNOWLEDGMENTS 57

VITA 58

LIST OF TABLES AND FIGURES

TABLE PAGE

I. Physical Constants 59

II. Constants Used in Equations of Appendix A for Determining Transfer Angles and Times 60

FIGURE

1. Illustration of Encounter involving increase in Vehicle velocity 61

2. Illustration of various phases of typical Flyby mission . . 62

3. Geometry used to initiate Pre-Encounter orbit at Earth . . . 63

4. Geometry of Hyperbolic Encounter at Planet 64

5. Geometry used to establish transfer angles and times 65

6. Geometry used to establish Transfer times and angles for Post-Encounter phase of Mission 66

7. Geometry used to establish Earth and Planet position with respect to Post-Encounter Aphelion and Perihelion 67

8. Geometry used to define necessary conditions for Encounter and for showing how the approach conditions determine if Encounter is Retrograde or Direct 68

9. Characteristics of direct transfer orbits 69

   (a) Perihelion distance and transfer time from insertion to perihelion for various launch velocities ($\theta_1 = 0$). 69

FIGURE PAGE

(b) Aphelion distance and transfer time from insertion to aphelion for various launch velocities (Θ_i = 180). 70

10. Post-encounter perihelion and transfer time from insertion to perihelion for various launch velocities and planetary approach conditions at Venus 71

11. Flyby orbits at Venus for direct and retrograde encounters . 72

12. Post-encounter perihelion attainable for various launch velocities and flyby distances at Venus 73

13. Mission time and Earth position with respect to post-encounter perihelion for various launch velocities and flyby distances at Venus 74

14. Post-encounter perihelion attainable for various launch velocities and flyby distances at Jupiter 75

15. Encounter orbits at Jupiter for different values of flyby distance 76

16. Transfer time from insertion to perihelion for various launch velocities and flyby distances at Jupiter 77

17. Earth position with respect to post-encounter perihelion for various launch velocities and flyby distances at Jupiter . 78

18. Maximum heliocentric velocity attainable via flyby at Jupiter at various distances of closest approach 79

19. Geometry used to establish approach corridor at planet activity sphere and corridor at perigee 80

FIGURE PAGE

20. Variation in approach and perigee corridors with percent of minimum perihelion achieved for Venus flyby-solar probe missions 81

21. Variation in approach and perigee corridors with percent of minimum perihelion achieved for Jupiter flyby-solar probe missions 82

a) Corridors for flyby distance greater than 6 planetary radii (fig. 14) 82

(b) Corridors for flyby distance less than 6 planetary radii (fig. 14) 83

22. Variation in Jupiter approach and perigee corridors with launch velocity for flybys which achieve solar impact . . 84

23. Variation in flyby parameters with distance of closest approach at Jupiter for the V_{he} = 10.8 km/sec condition yielding maximum encounter corridors (fig. 22) 85

ANALYSIS OF GRAVITY ASSISTED TRAJECTORIES FOR SOLAR-PROBE AND DEEP-SPACE MISSIONS

By John W. Young

INTRODUCTION

As planetary missions become more advanced the energy requirements and trip times become increasingly large for vehicles following direct transfer orbits from Earth. For example, a solar impact probe requires a velocity at the Earth activity sphere (hyperbolic excess velocity) of nearly 30 km/sec, while an escape orbit from the solar system would require a hyperbolic excess at Earth of 12.4 km/sec. An alternate approach to these direct-type transfers made feasible by recent advances in orbit determination and vehicle control, is to use the free energy attainable by passing through the gravitational field of an intermediate planet. This maneuver is commonly referred to as "Planetary Flyby" or "Hyperbolic Encounter." For example, proper utilization of the gravity field of Jupiter can reduce the required hyperbolic excess velocity for solar impact by a factor of three over that for a direct transfer. An analogous maneuver can reduce the required velocity for an escape from the solar system by nearly one third.

The general concept of planetary flyby can be stated briefly as follows. Consider a vehicle proceeding along a trajectory in heliocentric space. For certain orbits the vehicle may approach a passing planet such that the planetary gravity field exerts the primary perturbative force on the vehicle. While the vehicle orbit about the sun is

elliptic, the approach and departure with respect to the planet is along a hyperbolic path. This hyperbolic encounter can change the energy and angular momentum of the vehicle with respect to the sun. For example, consider the situation shown in figure 1. The vehicle enters the planet activity sphere with a heliocentric velocity, V_{1s}, and a relative velocity with respect to the planet, V_{1p}, such that it passes behind the planet (direct encounter). After having been deflected by the planet gravity field, the vehicle departs on a new orbit with heliocentric velocity, V_{2s}. Since the velocities of approach (V_{1p}) and departure (V_{2p}) with respect to the planet are equal, the encounter results in an increase in heliocentric velocity for the vehicle, as is seen in figure 1. A reverse type maneuver (retrograde), for which the vehicle passes in front of the planet, can result in a decrease in heliocentric velocity for the vehicle. Energy, of course, is conserved during a flyby since the orbit of the perturbing planet is altered in proportion to the masses involved in the encounter.

Numerous studies relating to planetary flyby have been made in the past, as will be outlined in a later section of this report. The objective of the present analysis is to supplement these studies by investigating various aspects of the flyby concept which were generally not emphasized in previous studies. An additional aim is to analyze in detail various flyby orbits to obtain an understanding of the basic mechanics involved.

Two types of flyby missions will be investigated. One such mission is the solar probe, with the objective of either achieving a solar impact

or of placing the vehicle in close proximity to the solar surface. The other type mission studied is the Deep Space mission. The objective of this mission is to either escape from the solar system or to achieve an aphelion distance greater than that possible without employing the flyby concept.

Results will be presented to illustrate the relative effects of various perturbing bodies on significant orbital variables such as transfer time, momentum and energy changes at the perturbing planet, and launch velocity requirements at Earth. Included will be an analysis of the effect on over-all mission performance of varying such flyby parameters as approach and departure direction and velocity and distance of closest approach (perigee) at the perturbing body. Consideration will be given to determining the sensitivity of specified orbital parameters to small variations in certain launch and approach conditions with the objective of establishing those quantities most critical to mission success.

In addition to the parametric type results previously outlined, an iterative, numerical procedure will be used to obtain a limited number of optimal missions. This procedure enables such trajectory variables as perihelion and aphelion distances following encounter or orbital transfer time to be either minimized or maximized subject to constraints on appropriate orbital parameters. Constraints could include launch energy and orientation of the transfer orbit at Earth, transfer angle and time, or certain approach and departure conditions at the perturbing body. These optimal missions are of practical importance for energy or

time limited missions and are of academic interest since they give insight into the basic concepts involved in planetary flyby.

Although a complete analysis of the mechanics of planetary flyby will be given in a later section, the technique applied in the present study can be briefly stated as follows. Since no analytical solution to the three-body problem exists, and since numerical integration of the three-body equations of motion is very time consuming, a two-body analysis was used. Thus, during a mission it was assumed that the vehicle trajectory was influenced by only one body at any particular time. Therefore, a typical mission consisted of three distinct segments, an initial heliocentric transfer from Earth to the activity sphere of the perturbing planet, a swingby of the planet under the influence of only the planetary gravity field, and a final heliocentric transfer to the desired destination.

NOTATION

a, b, c, e	semi-major and semi-minor axes, linear eccentricity and eccentricity of transfer orbits
Cr_{p_f}	perigee corridor at encounter planet (eq. (21))
$C\rho_a$	approach corridor at encounter planet (eq. (20))
E	eccentric anomaly
h	orbital energy constant
H	auxiliary angle of hyperbolic orbit
$K_1, K_3, \ldots, K_6$	constants
M	mean anomaly
r	radial distance
t	time
U	orbital velocity
V	velocity
V_{he}	hyperbolic excess velocity of vehicle at insertion
α	transfer angle associated with vehicle orbit
γ	elevation angle of velocity vector with respect to local horizontal
η	true anomaly
θ_a	angle between vehicle-planet and vehicle-sun radius vectors (fig. 4)
θ_i	angle which specifies orientation of insertion orbit at earth (fig. 3)
$\delta n, \theta_1, \theta_2, \theta_3, \theta_4, \beta$	angles used in determining flyby parameters

μ	gravitational field constant
ρ	radius of activity sphere
ϕ	angle used in specifying earth and planet positions at various mission times
ψ	angle between vehicle-sun and earth or planet-sun radius vectors

Subscripts.-

A, P	aphelion and perihelion conditions
d	direct transfer orbit
H	refers to parameters of post-encounter orbit
i	insertion conditions
s	heliocentric reference
p	planet reference
E	conditions associated with earth
f	refers to parameters of hyperbolic flyby orbit
1	approach conditions at planet activity sphere
2	departure conditions at planet activity sphere

Multiple subscripts.- When dealing with static quantities such as velocity, angular orientation, or radial distance, the first subscript generally denotes an initial reference position while the second subscript specifies the location to which this position is referred. For example, consider:

V_{1s} = heliocentric approach velocity at planet activity sphere (1 denotes approach condition, s denotes heliocentric reference)

η_{2s} = true anomaly of heliocentric departure orbit at planet activity sphere.

For quantities such as transfer angles and times, the first and second subscripts denote respectively the initial and final reference positions. For example consider:

α_{i1} = transfer angle from insertion to encounter

t_{i1} = transfer time from insertion to encounter

SURVEY OF LITERATURE

A comprehensive review of the mechanics of the flyby maneuver, as well as problems associated with the practical application of such a mission is given in reference 1. An interesting result of reference 1 is that, based on orbit determination and trajectory control procedures available at that time, it was concluded that certain applications of the flyby mission were impractical.

The advent of improved space navigation and guidance techniques has largely overcome the difficulties outlined in reference 1 and has lead to a renewed interest in flyby type missions. Since this renewed interest has resulted in a large volume of literature relating to the dynamics of, and requirements for planetary flyby, the present survey will be limited to typical studies covering the broad spectrum of available literature. In addition to these references relating to the dynamics of planetary flyby, literature will also be cited which details the mathematics involved in the optimization procedure employed in the present analysis.

References 2 and 3 present results which illustrate the advantages of, and requirements associated with the use of the flyby concept as applied to specific space missions. Reference 2 gives a general analysis of the use of the flyby concept for achieving a multi-planet flyby mission during the 1976-1979 time period. It is shown in reference 2 that the Grand Tour mission is feasible within projected state-of-the-art capabilities. Reference 3 discusses the requirements associated with round trip, Mars stopover missions which employ a Venus swingby technique.

The results are compared with those of a direct Mars mission for launch opportunities between 1980 and 1999. The results show that, in nearly all cases, the flyby significantly reduces the launch requirements at Earth.

Reference 4 presents an analysis of flyby missions of the type considered in the present study. A Lagrange multiplier procedure was also used to obtain various optimal missions. While a more complete physical model was used in reference 2 than in the present study (planet ephemeris as well as out-of-ecliptic transfers were included), the results were of a more specific nature since transfers were limited to those associated with particular Earth launch opportunities. It also appears that the constraints imposed on some transfer orbits lead to an omission of certain significant results.

An analysis of the use of a flyby of Jupiter for achieving Earth to Saturn missions is given in reference 5. Results were given to illustrate the increased payloads available using a flyby at Jupiter.

Reference 6 compares navigational and system capabilities with mission requirements for missions such as those of references 2 - 5 as well as those of the present analysis. It concludes that relatively simple supplements to present navigational systems can achieve the accuracies required for flyby missions.

The numerical optimization procedure used in the present analysis is based generaly on the accelerated gradient method for parameter optimization presented in reference 7. This reference outlines the basic theory involved in the optimization procedure. Additional studies which

present detailed analyses of various aspects of the optimization procedure are given in references 8, 9, 10, and 11.

Implementation of the actual computer program, as evolved from the techniques of references 7 - 11, was due largely to the efforts of I. L. Johnson (ref. 7) at the Manned Spacecraft Center, NASA. However, as no references are currently available in the literature, details concerning the computer program and its current application can be obtained on request from the author to the present report.

THEORY

Before proceeding with a development of the governing equations of the present analysis, a general description of the overall planetary flyby concept will be given to illustrate the various phases involved and to introduce the terminology to be used. A typical flyby mission is shown schematically in figure 2. While figure 2 depicts a flyby of a planet inside the Earth orbit for which the objective was to achieve a reduced perihelion distance, the various phases are similar for other missions considered in the study.

As shown in figure 2, the initial phase involves a heliocentric transfer from Earth to the perturbing planet. This transfer, which will be referred to as the pre-encounter orbit, is established by specifying the energy and orientation of the departure trajectory at the Earth activity sphere. This departure from Earth will be referred to as insertion. The second phase begins with the entry of the vehicle into the activity sphere of the planet. The planetary approach conditions are determined from the pre-encounter transfer orbit and from the assumed orientation of the vehicle with respect to the planet upon entry into its activity sphere. Following a hyperbolic swingby of the planet, the final phase begins as the vehicle exits the planet activity sphere. This phase, which will be referred to as the post-encounter orbit, consists of a heliocentric transfer to the final destination. Orbital parameters for the post-encounter phase are determined from exit conditions at the perturbing planet.

The assumptions and limitations of the present analysis as well as the physical and mathetical relationships used in the various phases shown on figure 2 will now be given.

Assumptions

Since the present study is of a general nature as opposed to specific studies previously cited in the SURVEY OF LITERATURE, certain simplifying assumptions were made. Planet ephemeris was not included and planets were assumed to move about the sun in circular orbits. In addition the orbit of planets, as well as all transfer maneuvers, were assumed to be coplanar. To reduce computational time, a two body analysis was assumed for all orbital transfers. Thus, a typical flyby mission consisted of a series of "patched conics", such that the vehicle was influenced by a single gravity field during any particular segment of a mission. The assumed physical constants for the planets are given in table I.

Due to the large number of missions available for consideration, certain limiting assumptions were also necessary. Only flybys of the planets Venus and Jupiter were included. Insertion at Earth was limited to directions either along ($\Theta_i = 180^\circ$) or opposed ($\Theta_i = 0^\circ$) to the Earth orbital direction. Thus, at insertion, the vehicle was near the aphelion position of the pre-encounter orbit during transfers to Venus. Likewise, transfers to Jupiter were initiated near perihelion on the pre-encounter orbit. These conditions are near optimal from an energy exchange standpoint. One additional limitation on transfer orbits was made to reduce the spectrum of possible missions. Pre-encounter orbits were limited

to transfer angles of less than 180°. Thus, Venus encounters occurred before the perihelion position of the pre-encounter orbit was reached, while Jupiter encounters were pre-aphelion.

Pre-Encounter Transfer Orbit from Earth

The geometry used to establish the transfer orbit from Earth to the perturbing planet is shown on figure 3. The orbit is determined by specifying the hyperbolic excess velocity vector at Earth. Thus, for assumed values for velocity magnitude and direction (V_{he} and Θ_i) at the Earth activity sphere, the required conditions for the heliocentric orbit can be determined as follows.

Initial conditions at Earth.- Vehicle distance from the sun at Earth is determined by applying the cosine law

$$r_i^2 = r_{Es}^2 + \rho_E^2 - 2r_{Es}\rho \cos(90 - \Theta_i)$$

Thus

$$r_i = (r_{Es}^2 + \rho_E^2 - 2r_{Es}\rho_E \sin \Theta_i)^{1/2} \tag{1}$$

Using the law of sines, the angular displacement of the vehicle from the Earth-sun line is

$$\frac{\sin \psi_i}{\rho_E} = \frac{\sin (90-\Theta_i)}{r_i}$$

or

$$\psi_i = \sin^{-1} \left(\frac{\rho_E \cos \Theta_i}{r_i}\right) \tag{2}$$

The heliocentric velocity and flight path angle of the vehicle, as shown in figure 3, is given by applying the cosine law

$$V_i = (V_{he}^2 + U_E^2 - 2V_{he}U_E \cos \Theta_i)^{1/2} \tag{3}$$

and

$$\gamma_i = - \sin^{-1}\left(\frac{V_{he}\sin \Theta_i}{V_i}\right) - \psi_i \tag{4}$$

<u>Orbital parameters for pre-encounter transfer</u>.- Using the previously established initial conditions for the transfer ellipse, the characteristics of the orbit can be established. Perihelion and aphelion conditions can be determined by applying conservation of energy and angular momentum. Conservation of energy yields

$$\frac{V_i^2}{2} - \frac{\mu_s}{r_i} = \frac{V_{P_d}^2}{2} - \frac{\mu_s}{r_{P_d}} \tag{5}$$

conservation of angular momentum gives

$$V_i r_i \cos\gamma_i = V_{P_d} r_{P_d}$$

or

$$r_{P_d} = \frac{V_i r_i \cos \gamma_i}{V_{P_d}} \tag{6}$$

Equations (6) and (5) yield

$$\frac{V_i^2 - 2\mu_s}{r_i} = \frac{V_{P_d}^2 - 2\mu_s V_{P_d}}{(V_i r_i \cos \gamma_i)}$$

or

$$V_{P_d}^2 - \left[\frac{2\mu_s}{V_i r_i \cos\gamma_i} \frac{V_{P_d} - V_i^2 - 2\mu_s}{r_i}\right] = 0$$

Thus, vehicle velocity at perihelion for a direct transfer from Earth is given by

$$V_{P_d} = \frac{\mu_s}{V_i r_i \cos\gamma_i} + \left[\left(\frac{\mu_s}{V_i r_i \cos\gamma_i}\right)^2 + \frac{V_i^2 - 2\mu_s}{r_i}\right]^{1/2} \tag{7}$$

using this value for V_{P_d}, the perihelion distance is found from equation (6).

In a similar manner aphelion velocity and distance for a direct transfer from Earth, can be found to be

$$V_{P_d} = \frac{\mu_s}{V_{P_d} r_{P_d}} - \left[\left(\frac{\mu_s}{V_{P_d} r_{P_d}}\right)^2 + \frac{V_{P_d}^2 \quad 2\mu_s}{r_{P_d}}\right]^{1/2} \tag{8}$$

$$r_{A_d} = \frac{r_{P_d} V_{P_d}}{V_{A_d}} \tag{9}$$

Standard conic relationship (reference 1) for the semi-major and semi semi-minor axes and the numerical and linear eccentricities of the transfer ellipse are given in equations (A-3) of Appendix A.

Hyperbolic Encounter at Planet

The planetary flyby phase of a mission included the approach to encounter at the activity sphere of the perturbing body, the hyperbolic orbit about the planet, and the exit from the planet following encounter. The equations defining vehicle motion during these portions of the flyby will now be developed using the geometry of figure 4.

Approach conditions at planet activity sphere.- The technique used to establish approach conditions at the planetary activity sphere was to first establish heliocentric conditions at this point and then to transfer from a solar to a planetary reference system. The orientation of the approach orbit on the activity sphere of the planet, which is needed to calculate vehicle radial distance from the sun, was specified by assuming a value for the angular displacement (θ_a) between the vehicle-sun and vehicle-planet radius vectors. As will be shown in a later section of the report, an assumed value for Θ_a in effect determines the transfer time from insertion to encounter and thus establishes the launch date or angular separation of the planet and Earth at insertion.

As shown in figure 4, the angle between the vehicle-sun (r_{1s}) and planet-sun(r_{ps}) radii is given by

$$\psi_{1s} = \sin^{-1}\left(\frac{\rho_p \sin \theta_a}{r_{ps}}\right) \tag{10}$$

The radial distance of the vehicle from the sun is now given by

$$r_{1s}^2 = r_{ps}^2 + \rho_p^2 - 2r_{ps}\,\rho_p \cos\left[180^\circ - (\psi_{1s} + \theta_a)\right]$$

or

$$r_{1s} = \left[r_{ps}^2 + \rho_p^2 + 2r_{ps}\,\rho_p \cos\left(\psi_{1s} + \theta_a\right)\right]^{1/2} \tag{11}$$

Applying conservation of energy and angular momentum for the pre-encounter orbit, the heliocentric velocity and flight path angle at the activity sphere are given by

$$V_{1s} = \left[V_i^2 + 2\mu_s \frac{1}{r_{1s}} - \frac{1}{r_i}\right]^{1/2} \tag{12}$$

and

$$\gamma_{1s} = K_2 \cos^{-1}\left[\frac{V_i r_i \cos\gamma_i}{V_{1s} r_{1s}}\right] \tag{13}$$

where K_2 is determined by the pre-encounter orbit, as will be explained in a later section of the report.

A coordinate change from a heliocentric to a planetary reference can now be made for the vehicle orbit. From figure 4 it is seen that the relative velocity of the vehicle with respect to the planet is

$$V_{1p} = \left[U_p^2 + V_{1s}^2 - 2U_p V_{1s} \cos(\psi_{1s} - \gamma_{1s})\right]^{1/2} \tag{14}$$

also

$$\theta_2 - \gamma_{1p} + \theta_a + \psi_{1s} = 180^\circ$$

where

$$\theta_2 = \sin^{-1}\left(\frac{V_{1s} \sin(\psi_{1s} - \gamma_{1s})}{V_{1p}}\right)$$

thus

$$\gamma_{1p} = \theta_a + \psi_{1s} + \theta_2 - 180^\circ \tag{15}$$

Hyperbolic orbit at perturbing planet.- Having determined the velocity and flight path angle of the vehicle with respect to the planet, the procedures of equations (5) through (9) yield the perigee condition at the planet. These are given in equations (A-6) of appendix A. Standard conic relationships (ref. 1) for the semi-major and semi-minor axes, numerical and linear eccentricities, and the true anomaly of the vehicle are given in equations (A-7) and A-8) of appendix A.

Departure conditions at planet activity sphere.- Since the hyperbolic approach and departure conditions with respect to the planet must be the same we have

$$V_{2p} = V_{1p}, \ \gamma_{2p} = -\gamma_{1p}$$

In order to determine the orbital parameters for the post-encounter transfer orbit, a change must be made from a planet to a solar reference system. Referring to figure 4 we have for the vehicle distance to the sun

$$r_{2s}^2 = \rho_p^2 + r_{ps}^2 - 2\rho_p r_{ps} \cos(\theta_3 - 90^\circ)$$

where

$$\theta_3 = 2\eta_{1f} - \theta_1$$

and

$$\theta_1 = 90^\circ - \psi_{1s} - \theta_a$$

thus

$$r_{2s} = \left[\rho_p^2 + r_{ps}^2 + 2\rho_p r_{ps} \cos \beta\right]^{1/2} \tag{16}$$

where

$$\beta = 2\eta_{1f} + \theta_a + \psi_{1s}$$

From figure 4 it is seen that the angle between the planet-sun and vehicle-sun lines is given by

$$\frac{\sin \psi_{2s}}{\rho_p} = \frac{\sin(\theta_3 - 90^\circ)}{r_{2s}} = - \frac{\cos \theta_3}{r_{2s}}$$

or

$$\psi_{2s} = - \sin^{-1}\left[\frac{\rho_p}{r_{2s}} \sin \beta\right] \tag{17}$$

Figure 4 shows that the heliocentric velocity of the vehicle following encounter is given by

$$V_{2s}^2 = V_{2p}^2 + U_p^2 - 2V_{2p}U_p \cos\left[\gamma_{2p} - (\theta_3 - 90^\circ)\right]$$

or

$$V_{2s} = \left[V_{2p}^2 + U_p^2 + 2V_{2p}U_p \cos(\beta - \gamma_{2p})\right]^{1/2} \tag{18}$$

The heliocentric flight path angle, γ_{2s}, can be found from figure 4 as follows

$$\frac{\sin\left[\gamma_{2p} - (\theta_3 - 90^\circ)\right]}{V_{2s}} = \frac{\sin(- \gamma_{2s} - \psi_{2s})}{V_{2p}} = \frac{\cos(\theta_3 - \gamma_{2p})}{V_{2s}}$$

or

$$- \sin(\gamma_{2s} + \psi_{2s}) = \frac{V_{2p}}{V_{2s}} \cos(2\eta_{1f} - 90^{\circ} + \psi_{1s} + \theta_a - \gamma_{2p})$$

thus

$$\gamma_{2s} = - \sin^{-1}\left[\frac{V_{2p}}{V_{2s}} \sin(\beta - \gamma_{2p})\right] - \psi_{2s} \tag{19}$$

Post-Encounter Transfer Orbit

The post-encounter orbit is, respectively, elliptical, parabolic, or hyperbolic as the orbital energy constant, h_{2s}, is negative, zero, or positive. For elliptic orbits the perihelion and aphelion conditions can be determined as was previously done in equations (5) through (9). For parabolic or hyperbolic orbits, an escape from the solar system is achieved. The conditions which determine the nature of the post-encounter orbit are listed in appendix A and the governing equations and conic relationships for the orbit are given in equations (A-11) and (A-12).

Transfer Times and Angles

Various transfer times and angles of interest for flyby missions under consideration will now be established with the aid of figure 5.

Heliocentric transfer from Earth to planet inside Earth orbit.- Transfers to planets inside the Earth orbit were limited to cases for which insertion at Earth occurred at or past aphelion (r_{A_d}) on the transfer orbit. Thus, the true anomaly (η_i) of the vehicle at insertion is less than 180° and the vehicle is initially on the descending leg of

the transfer ellipse (negative γ_{1s}). The various transfer angles, times, and initial positions of the Earth and planet at insertion and encounter are easily obtained from figure 5, and are given in equations (A-13) - (A-18) of appendix A. Note from equations A-4, A-13, A-16, and A-18 that by fixing Θ_a, the launch date or angular separation of the planet and Earth at insertion is established.

Heliocentric transfer from Earth to planet outside Earth orbit.- Transfers to planets outside the Earth orbit were limited to cases for which insertion at Earth occurred at or past perihelion (r_{P_d}) on the transfer orbit, as is shown in figure 5. Thus, the vehicle at insertion was on the ascending portion of the transfer ellipse (+ γ_{1s}). The geometry involved for these types of transfers is given in figure 5 and the various relationships of interest are listed in equations (A-13) - (A-18) of appendix A.

Post-encounter transfer orbit.- As was previously stated, the post-encounter orbit is dependent on the orbital energy constant h_{2s}, being elliptic, parabolic, or hyperbolic as h_{2s} is, respectively, negative, zero, or positive. Since an escape from the solar system is achieved if the post-encounter transfer is hyperbolic or parabolic, no transfer angles or times were computed for these orbits.

Two possibilities exist for elliptic post-encounter orbits since the heliocentric flight path angle (γ_{2s}) can be either positive or negative. The geometry used to establish the transfer angles and times for this phase of a mission is given in figure 6. Transfer angles and times for the post-encounter orbit are given in equations (A-22) and (A-23) of appendix A.

Transfer time from insertion at Earth to the perihelion or aphelion position on the post-encounter orbit is obtained by summing the individual times for each phase of the mission and is given in equations (A-24) of appendix A.

Flyby maneuvers result in a displacement of the major axis of the post-encounter transfer orbit from that of the direct transfer orbit. It is of interest to establish this displacement in order to determine the positions of the Earth and planet with respect to post-encounter perihelion and aphelion. The geometry used in defining this is given on figure 7 and the desired equations are given in (A-25) of appendix A.

The equations developed in preceding sections of this report and the required standard conic relationships are summarized in appendix A. While these equations define vehicle motion from insertion at Earth to aphelion or perihelion on the post-encounter orbit, certain constraints must be applied to the pre-encounter orbit in order to achieve a desired encounter. These conditions will now be outlined.

Necessary Conditions at Insertion and Encounter

Insertion conditions.- An obvious constraint on insertion conditions is that the pre-encounter orbit must intersect the orbit of the planet with which an encounter is desired. Thus, for encounters with a planet inside the Earth orbit, the perihelion (r_{P_d}) of the transfer orbit must be less than the planet-sun radial distance (r_{ps}). Likewise, for encounters with planets outside the Earth orbit, the aphelion (r_{P_A}) of the transfer orbit must be greater than r_{ps}. Hence, the hyperbolic excess velocity vector (V_{he}) at Earth must be such that the preceding

conditions are fulfilled. These conditions are given in (A-26) of appendix A.

Encounter conditions.- Constraints on encounter conditions at the activity sphere of the perturbing planet will be defined with the aid of figure 8. This figure shows how the vehicle is postioned with respect to the perturbing planet by specifying the angle (θ_a) between the vehicle-planet and vehicle-sun lines. Thus, for values of θ_a between 0 and and 180°, the approach is in quadrant I ($0 \leq \theta_a \leq 90^\circ$) or quadrant II ($90^\circ \leq \theta_a \leq 180^\circ$) of figure 8; while for larger values of θ_a the approach is in quadrant III ($180^\circ < \theta_a \leq 270^\circ$) or quadrant IV ($270^\circ < \theta_a < 360^\circ$).

From figure 8 it is seen that for an encounter to occur, the heliocentric conditions for the vehicle must be such that an entry is made into the activity sphere of the planet: Thus, the relative velocity of the vehicle with respect to the planet (V_{1p}) must be directed into the activity sphere ($-180^\circ < \gamma_{1p} < 0$). These encounter conditions are listed in (A-27) of appendix A.

It should be noted that, if the flight path angle of the flyby orbit (γ_{1p}) is equal to -90°, an impact with the planet will result. Thus, the magnitude of γ_{1p} determines whether the encounter is retrograde or direct and the limiting values for each quadrant is apparent from figure 8. For example, a retrograde maneuver occurs for quadrants I and IV if, γ_{1p} is between 0 and -90° while a direct encounter would result in quadrants II and III for the same approach conditions.

RESULTS AND DISCUSSION

The results to be presented were, as previously stated, obtained by two methods. One method consisted of parametrically varying launch energy and orientation (Θ_i, V_{he}) and approach angle (Θ_a) at the activity sphere of the encounter planet. The second method of analysis made use of a numerical optimization procedure to obtain values for the launch and approach variables such that some orbital function was optimized subject to constraints on other orbital parameters.

It should be stated that, while the results could have been obtained without reliance on the optimization computer program, its' use greatly reduced the data collection task. For example, a specific flyby mission satisfying certain criterion can be obtained with a single computer run using the optimization program. This same mission might otherwise require a large number of runs with a resultant lengthy data reduction effort needed to obtain the desired flyby result. Thus, the optimization program was, in general, used to reduce computer and data reduction time by establishing nominal values for mission variables. The variables were then varied parametrically about these nominal values.

In the following presentation of results no distinction will be made regarding the method of data collection.

Direct Transfer Orbits from Earth

Direct transfer orbits from Earth were determined to provide an index for comparison of the performance of planetary flyby missions as well as to establish possible pre-encounter orbits. Parameters of interest for these direct transfers are given in figure 9.

Shown on figure 9(a) is the perihelion distance and time from insertion to perihelion for various values of hyperbolic excess velocity at Earth. As previously stated, these transfers inside the Earth orbit were established by inserting the vehicle in a direction opposite to the Earth's orbit ($\theta_i = 0$). Note that insertion velocities of at least 2.5 km/sec are required for encounters at Venus.

Figure 9(b) gives the aphelion distance and transfer time for launches outside the orbit of the Earth. For these transfers, the insertion angle (θ_i) was 180°. Note that launch velocities of nearly 9 km/sec are required to effect an encounter at Jupiter. Due to the strong influence of launch energy for these transfers, a wide variation in transfer time to aphelion occurs, as is seen on figure 9(b).

Solar Probe Missions

Results were obtained for solar probe type missions which involved intermediate flybys of Venus and Jupiter. The objectives were to determine the influence on overall mission performance of various launch (V_{he}, θ_i) and planetary approach (θ_a) conditions. An additional aim was to establish areas of interest with respect to mission optimization and to define criterion for evaluation of these optimal type missions.

Venus flyby.- The basic nature of a flyby orbit at Venus will be illustrated with the use of figures 10 and 11. Shown on figure 10 is the post-encounter, perihelion distance, and the transfer time from insertion to perihelion for various launch and Venus approach conditions. The vehicle was inserted at Earth in a direction opposite the Earth's orbital

direction ($\theta_i = 0$), and the encounter condition was pre-perihelion (see fig. 5). As is seen on figure 10, perihelion and transfer time are strongly influenced by the approach condition. The discontinuity in the curves represents conditions for which an impact at Venus occurs.

Consider the variation of perihelion distance with θ_a given on figure 10 for $V_{he} = 6$ km/sec. As θ_a is increased from zero, perihelion increases from the direct transfer value of about 0.468 AU to about 0.6 AU for $\theta_a = 9.5^\circ$. For this range of approach conditions, the encounter is direct (see fig. 1). The increase in r_{P_H} with θ_a is a result of the vehicle approaching closer and closer to the planet surface as θ_a approaches its limiting value of 9.5°. This limiting value represents the condition for which the vehicle passes the planet at a distance of one planetary radii (6200 km). While the one planetary radii limit was chosen for computational convenience, in an actual mission the approach would be limited to about 1.1 planetary radii so as to remain above the planet atmosphere and thus prevent possible contamination or impact with the planet.

As θ_a is further increased, the encounter orbit passes from one side of the planet to the other, and at $\theta_a = 11^\circ$ the distance of closest approach is again one planet radii. For this condition, the encounter is retrograde and a minimum value for perihelion is achieved. For large values of θ_a, flyby distance increases and r_{P_H} approaches the direct encounter condition. The upper limit for θ_a of about 85° shown on figure 10 corresponds to the condition for which the vehicle just intersects the activity sphere of the planet. For larger values of θ_a, encounters are not possible.

As is shown on figure 10, an increased launch velocity yields a reduced perihelion. The transfer time curves shown on figure 10 illustrate a basic fact associated with most physical problems. That is, increased performance with respect to one variable must generally come at the expense of some other variable. For example, as seen on figure 10, a reduced perihelion yields an increased transfer time and vice versa.

Consider again the two limiting cases for direct ($\theta_a = 9.5^o$) and retrograde ($\theta_a = 11^o$) encounters shown on figure 10. To obtain a physical picture of the mechanics involved, it is instructive to examine the actual flyby orbits for the two cases. This is illustrated schematically on figure 11 for the two limiting encounters. Given are the approach and departure conditions at the planet activity sphere, as well as additional flyby parameters. While radius vectors given on figure 11 cannot be shown to scale, velocities and angles are properly scaled. Note that the encounter conditions for both cases are almost the same, the only significant difference being that elevation angle (γ_{1p}) for the direct or retrograde cases is respectively slightly greater than or less than 90°. Thus, in the direct encounter the vehicle passes behind the planet while for the retrograde case the vehicle passes in front of Venus.

While approach angle to the planet (θ_a) is a convenient variable mathematically for establishing the encounter orbit, a more practical parameter for evaluating the orbit is the distance of closest approach (r_{p_f}) to the planet. Shown on figure 12 is the solar perigee attainable

as a function of distance of closest approach at Venus for various launch velocities at Earth. For comparison purposes, the perihelion distance for direct transfers from Earth is also given. From this figure it is seen that as the distance of closest approach at Venus is reduced, the post-encounter perihelion is also reduced, with a maximum decrease of about 65 percent (over that for the direct launch) occurring at a flyby perigee of one planetary radius.

Total mission time to perihelion and Earth position with respect to perihelion are given on figure 13 for the range of conditions included on figure 12. For comparison, direct transfer conditions are also included. As shown, the flyby maneuver only slightly effects total mission time. From a pratical standpoint, the increased times required for the flyby orbits would have little effect on overall mission performance.

The variation in Earth position with respect to post-encounter perihelion given on figure 13, is of practical importance since the Earth should be in a favorable position to receive telemetry transmission from the vehicle during perihelion passage. While the ideal condition might be for the Earth and vehicle to be aligned ($\phi_{EPH} = 0$), it is seen on figure 13 that line of sight contact is achieved for the conditions considered and that the increase in transmission distance is not excessive. For example, consider the values given for $V_{he} = 6$ km/sec and $r_{p_f} = 1$ planet radii. The increased transmission distance for the flyby mission is about 50 percent greater than that for the ideal case ($\phi_{EPH} = 0$) and only about 5 percent greater than for the direct transfer orbit.

Jupiter flyby.- In the preceding analysis of Venus flyby, solar-probe missions, the results presented followed a somewhat predictable pattern. However, since the gravitational field at Jupiter is much larger than that at Venus, solar-probe missions involving flybys at Jupiter are more interesting and unpredictable in nature, as will be shown in the following discussion.

Figure 14 shows the variation in solar perihelion with distance of closest approach at Jupiter for several values of launch velocity. The results of figure 14 were for a launch along the Earth orbital velocity vector ($\theta_i = 180^\circ$). In contrast to the results for similar flybys at Venus (fig. 12), minimum perihelion is not attained at the limiting flyby distance of one planetary radius and, for some launch velocities, multiple minima occur. Also, while the minimum perihelion for a Venus flyby was about 0.146 AU (V_{he} = 12 km/sec), solar impacts are actually attained for the minima shown on figure 14 associated with launch velocities of 11 and 12 km/sec. In order to explain the existence of multiple minima shown on figure 14, it is of interest to examine the basic mechanics of the flyby orbits involved. Consider the minima attained for V_{he} = 11 km/sec at distances of closest approach of 3.9 and 12.9 planetary radii. The encounter orbits are depicted on figure 15. The velocities and angles shown on figure 15 are to scale while the radial distances are not.

Note that encounter conditions are nearly the same for each orbits shown on figure 15, the only significant difference being that the initial flight path angle is about one degree nearer the vertical for

the closer flyby orbit. This closer approach gives a greater deflection angle at the planet with the result that, following the encounter, the vehicle's heliocentric velocity vector is practically aligned with the radius vector to the sun ($\gamma_{2s} \approx -90^{\circ}$). For the $r_{p_f} = 12.9$ case, the smaller deflection angle results in a positive heliocentric flight path angle of about 90° as shown on figure 15. Thus, the vehicle proceeds outward along the vehicle-sun line and then falls back into the sun.

A similar effect to that shown on figure 15 accounts for the minima shown on figure 14 for $V_{he} = 12$ km/sec. Note that for this case there are actually three values of r_{p_f} for which minima exist, with two values occurring for $r_{p_f} < 2$. These lower minima result as the post-encounter flight path angle (γ_{2s}) passes successively through -90° in an increasing and decreasing fashion. While the scale on figure 14 does not show it, a similar effect occurs on the $V_{he} = 11$ km/sec curve between values for r_{p_f} of 3 and 4 planet radii.

The single minima shown on figure 14 for launch velocities of 9 and 10 km/sec is due to a different effect from those previously described. These result not from the vehicle being directed either toward or away from the sun, but from a reduction in heliocentric velocity such as occurred for retrograde encounters at Venus (fig. 11).

A further examination of figure 14 shows that, for $V_{he} = 9$ km/sec, the direct transfer condition yields a lower perihelion than on the flyby orbit. Thus, only velocities of at least 10 km/sec will be included in further analysis of Jupiter, solar-probe missions.

Based on perihelion alone, the Jupiter flyby is far superior to the Venus flyby, as a comparison of figures 14 and 12 show. Also, for the

Jupiter case, solar impacts can be achieved at greater flyby distances, thus reducing the risk of planetary impact. Again, considering only perihelion, the minima corresponding to flybys at about 14 planetary radii are preferable to those at closer flyby distances. However, a complete evaluation of the Jupiter, solar-probe mission must include an analysis of other significant trajectory variables.

An important factor for flyby missions is the total trip time. Mission times for the encounter conditions discussed in figure 14 are given on figure 16. This figure shows that, for the launch velocities included, time from insertion to perihelion increases almost linearly with distance of closest approach at Jupiter. Thus, for $V_{he} = 12$ km/sec, mission time increases from about 950 to 2900 days respectively for the flyby distances of 1.5 and 14.5 planetary radii corresponding to minimum perihelion conditions. Mission times of about 1050 and 1700 days occur for the lower and upper minima in the $V_{he} = 11$ km/sec case. This increase in mission time with flyby distance is in general, caused by the effect described on figure 15. That is, as r_{p_f} becomes greater, the post-encounter flight path angle (γ_{2s}) increases from negative to positive values such that the post-encounter orbit progresses from a pre-perihelion to a pre-aphelion condition.

Consider now the position of the Earth with respect to perihelion passage by the vehicle. This quantity, which is of practical significance from a telemetry standpoint, is shown on figure 17 for the Jupiter flyby missions in question. Since this displacement angle increases nearly linearly with time, for simplicity only the magnitude of the

angle and those values near minimum perihelion are included on figure 17. Positive angle displacements from perhelion are found on the negative slope portion of the curves on figure 17.

Consider the V_{he} = 12 km/sec data of figure 17. Note that for the close planet flyby situation, the Earth and vehicle are at near opposition during minimum perihelion conditions. Thus, telemetry transmission would be impractical in this region. The close flyby, minimum perihelion conditions for V_{he} = 11 km/sec are seen to yield very vavorable telemetry conditions. To a somewhat lesser degree, this is also true for all minimum perihelion orbits at the larger flyby distances (r_{p_f} > 11 planet radii).

An analysis of the Jupiter flyby, solar-probe mission based on the data of figures 14, 16, and 17; that is, distance of closest approach to the planet, mission time, and Earth position at perihelion passage, leads to the following conclusions. As previously stated, from a consideration of reduced risk of impacting the planet, flyby distances greater than about 11 planetary radii are desirable (fig. 14). Telemetry transmission conditions are also favorable for these flyby distances (fig. 17). However, the increased times required for these missions (fig. 16), particularly for the highest energy launch, may necessitate flybys at the minimum perihelion conditions achieved for r_{p_f} < 5 planet radii. Under these circumstances, the lower energy launch (V_{he} = 11 km/sec) is preferable since a solar impact is achieved at a greater flyby distance in addition to having the Earth in a near ideal position for telemetry transmission. It is also of interest to note that, for the V_{he} = 11 km/sec launch, the perihelion curve is nearly flat for planet

approach distances between about 3 and 15 planet radii. Therefore, this transfer orbit would appear to be less sensitive than the others to errors in approach conditions. However, a final evaluation must include an error sensitivity analysis for the various flyby orbits. This analysis will be given in a later section of the report.

Deep Space Missions

In the present study, deep space type missions of a specific nature were not considered. The analysis was limited to establishing the maximum performance attainable for such missions through use of an intermediate flyby of Venus and Jupiter.

Venus flyby.- Various flyby orbits at Venus were computed to determine the maximum post-encounter aphelion attainable. The results, which were in agreement with reference 4, showed only marginal improvements over those for direct transfers from Earth. Thus, no data relating to Venus flyby - deep space missions is included in the present report.

Jupiter flyby.- In contrast to Venus flybys, encounters with Jupiter provide a definite advantage over a direct Earth launch for deep-space missions. This capability is shown in figure 18. This figure gives the maximum heliocentric velocity attainable following a direct encounter as a function of distance of closest approach at Jupiter and excess velocity at Earth. The heliocentric velocity which would result at the orbit of Jupiter on a direct transfer from Earth is also given for purposes of comparison.

Figure 18 shows that, for a wide range of flyby orbits, significant increases in heliocentric velocity are attainable. An escape from the

solar system is, in fact, achieved for the results shown on figure 18, since the solar system escape velocity at Jupiter is about 18 km/sec. The required direct launch velocity (V_{he}) at Earth to effect a solar system escape would be about 12.4 km/sec.

While detailed results relating to flybys at Jupiter for use in other outer solar system missions will not be given, one such comparison is of interest. Consider the case of a Saturn mission. A direct launch to Saturn would require a hyperbolic excess velocity at Earth of at least 10.4 km/sec. For this launch, the heliocentric velocity at Jupiters orbital distance would be about 13.5 km/sec. Thus, it is seen from figure 18 that a Saturn mission could be achieved with a launch velocity as low as 9 km/sec by using a Jupiter flyby.

A feature of interest on figure 18 is that the maximum post-encounter velocity occurs at a flyby distance of about 2 planet radii. This results since the deflection angle at Jupiter is such that the vehicle exits in a direction nearly aligned with the orbital velocity of Jupiter ($\gamma_{2s} \sim 0$). Thus, for this flyby distance, a maximum increase in heliocentric velocity is realized (see fig. 11).

Guidance Analysis for Flyby Missions

Various questions of practical significance arise in the analysis of results presented in previous sections of this report. An evaluation of the idealized data given may lead to premature conclusions regarding the relative merits of a particular mission. Thus, any final analysis must consider the guidance accuracy requirements as compared to that attainable with current state of the art techniques. In addition, the

sensitivity of critical orbital quantities to variations in launch and approach parameters must be included. A complete sensitivity study of the flyby concept as applied to particular mission applications would require a thorough error analysis and is beyond the scope of the present study. However, certain conclusions of a general nature regarding the guidance requirements for flyby missions can be made.

Approach corridor analysis.- A standard procedure for establishing the guidance requirements of a particular space mission is to specify a corridor width at some position on the transfer orbit. This corridor represents a "keyhole" through which the vehicle must pass to accomplish the desired mission. In any detailed analysis, the corridor at some point in space can be pictured as an "error ellipsoid". The axes of the ellipsoid would specify allowable deviations in position and velocity components. Since the present study is limited in scope, a simplified corridor analysis will be used.

Two accepted procedures for specifying planetary approach corridors are to give allowable deviations in either the vehicle position at some distance from the planet, or in the perigee distance achieved during passage at the planet. Both methods will be used in the present study.

Allowable deviations in position will be determined at the activity sphere of the planet. This corridor, which represents a segment of arc which must be intersected at the activity sphere by the vehicle orbit, is seen from figure 19 to be:

$$C\rho_a = \rho_a(\delta\theta_a + \delta\psi_{1s}) \tag{20}$$

where $\delta\theta_a$ is a small increment in the approach position on the activity sphere, and $\delta\psi_{1s}$ is the resulting change in vehicle-sun-planet angular displacement. The perigee corridor is merely the difference in perigee attained for the two approach conditions shown on figure 19 and is given by:

$$Cr_{p_f} = r_{p_f} - r'_{p_f} \tag{21}$$

where the unprimed and primed quantities refer respectively to the θ_a and $\theta_a + \delta\theta_a$ approach conditions.

This simplified representation neglects certain factors which would have to be considered in a more complete analysis. While the small increment in θ_a yields nearly identical flyby orbits, there are minute differences in the approach velocity and elevation angle (V_{1p}, γ_{1p}). Although inclusion of these small differences in approach conditions at the corridor limits would slightly alter the resulting corridors, the changes are insignificant as applied to the present study.

Venus encounter corridors.- Shown on figure 20 are variations in approach and perigee corridors at Venus with percent of minimum solar perihelion attained. Zero corridor conditions on this figure represent the case for which the vehicle passes Venus at a flyby distance of one planet radius (fig. 12). Thus, as the corridor increases, perihelion and flyby distance (r_{pf}) also increase. As seen on the figure, launch velocity at Earth has little effect on approach and perigee corridors at Venus.

From a practical consideration, figure 20 can be interpreted as follows. Assume that, for a particular solar probe mission; launch,

orbit determination, and guidance errors are such that the vehicle can be positioned on the activity sphere of Venus within a 4000 km distance of the aim point. Thus, to achieve minimum perihelion while avoiding an impact at Venus, the approach corridor ($C\rho_a$) would be 8000 km with the aim point being the 4000 km corridor condition. Likewise, the perigee corridor would be one planet radius in width with the aim point being at a flyby distance of 1.5 planet radii. For this situation, solar perihelion would be between 60 and 100 percent of the minimum achievable value.

As was shown in reference 6, expected accuracy in delivering the mariner-Venus probe was within a 100 x 250 km ellipse at the target aim point. This accuracy was to be achieved with only Earth based tracking and did not rely on on-board measurements which could be expected to further improve planet approach guidance. Thus, assuming similar approach guidance accuracy, figure 20 shows that a successful Venus flyby-solar probe mission could be achieved with at least 95 percent of minimum perihelion being attained.

Jupiter encounter corridors.- Figure 21 gives the variation in approach and perigee corridors with achievable solar perihelion for various launch velocities at Earth. The results shown are for conditions near the multiple minimum perihelion values occurring at flyby distances less than and greater than 6 planet radii (fig. 14).

Corridors associated with the larger flyby distances are given on figure 21(a). As before, zero corridors occur at the minimum perihelion condition shown on figure 14. Positively and negatively increasing

corridors refer respectively to flyby distances greater and less than the minimum perihelion flyby distance.

An analysis of figure 21(a) shows that the corridors decrease as launch velocity is increased. Positive corridors are seen to be somewhat larger than corresponding negative corridors. In contrast to Venus flybys (fig. 20) for which the aim point cannot be the zero corridor case, the optimal aim point for a Jupiter flyby would be at the zero corridor condition.

Shown on figure 21(b) are corridors for the lower flyby distance-minimum perihelion missions shown on figure 14. While previous figures have shown zero corridors at the 100 percent condition, figure 21(b) reveals a sizeable corridor width at this point. This results since the perihelion curves of figure 14 are fairly flat at the lower minimum flyby conditions and a solar impact is actually attained over a range or orbits about the minimum.

As seen on figure 21(b), the lower energy launch gives significantly larger approach and perigee corridors than for the higher energy launch. Also, the chance of planetary impact is greatly reduced for the V_{he} = 11 km/sec transfer since minimum perihelion is achieved at a greater flyby distance. Thus, consideration of flyby corridors, transfer times (fig. 16), and telemetry transmission conditions (fig. 17) reveals a distinct advantage for the lower (V_{he} = 11 km/sec) as opposed th the higher (V_{he} = 12 km/sec) energy transfer orbit.

In order to establish approach and perigee corridor conditions for which a solar impact is achieved, various flyby orbits were computed for launch velocities between 10 and 12 km/sec. The results are shown on

figure 22. The corridors given are equivalent to the 100 percent corridors shown on figure 21(b). Note that maximum corridor width occurs at a launch velocity of about 10.8 km/sec and that, for launch velocities as low as 10.5 km/sec solar impact is achieved with wider corridors than those for launch velocities greater than about 11 km/sec.

The variation of certain flyby parameters for the maximum corridor condition of figure 22 is of interest and is given on figure 23. Shown is solar perihelion distance, transfer time, post-encounter heliocentric flight path angle and velocity, and vehicle-Earth angular separation at perihelion passage for various flyby distances at Jupiter. An analysis of figure 23 shows why a solar impact is attained over such a wide range of flyby distances. For $r_{p_f} > 8.5$ and $r_{p_f} < 6.5$ planet radii, post-encounter flight path angles are close to $+90^\circ$ and -90° respectively. Thus, small perihelion values are attained. For encounter conditions such that $8.5 > r_{p_f} > 6.5$ the reduced perihelion results from low values for post-encounter, heliocentric velocity. This variation in V_{2s} and γ_{2s} results since the vehicle velocity vector with respect to Jupiter (V_{2p}) is nearly opposed to the planet velocity vector following encounter (see fig. 15).

It is apparent from previously given results that, with respct to overall mission performance, many tradeoffs exist between such flyby parameters as launch velocity, mission duration, encounter corridors, and telemetry transmission conditions. It is of interest to note that, for Jupiter flyby-solar probe missions, superior overall mission performance is attained with launch velocities less than the maximum assumed values.

The encounter corridor analysis has been limited to solar probe missions and has not included deep space type missions. No corridor analysis for deep space missions is included since the study of these transfers was limited to solar system escape orbits. Also, for this type mission, post-encounter conditions are fairly insensitive to flyby conditions, as was shown on figure 18. Had consideration been given to specific deep space missions than a guidance corridor analysis would be required. For example, a Jupiter flyby-Saturn mission with an objective of placing the vehicle between the rings of Saturn puts rather stringent limits on approach guidance.

SUMMARY AND CONCLUSIONS

A study has been made of the planetary flyby concept as applied to solar probe and deep space missions. The objectives were to supplement previous studies and to analyze various aspects of the flyby mission to acquire an understanding of the basic mechanics involved.

A planar two-body analysis was used in the study. Thus a typical mission consisted of a pre-encounter, heliocentric transfer from Earth to the activity sphere of the perturbing planet, a planet referenced flyby orbit, and a heliocentric transfer the final destination. An iterative, numerical procedure was used to obtain various optimal missions subject to constraints on appropriate orbital parameters. Variables included in the study were the energy and orientation of the launch trajectory at Earth and the approach direction to the perturbing planet. Hyperbolic excess velocities at Earth between 6 and 12 km/sec were used in the study.

Results are presented to illustrate the effect of flybys at Venus and Jupiter on such parameters as transfer time, momentum and energy changes at the perturbing planet, approach and flyby corridor widths, and conditions at perihelion passage with respect to possible telemetry transmission from the vehicle to Earth.

The results of the study can be summarized as follows:

1. Maximum reductions in perihelion of about 65 percent over that for direct transfers are possible for Venus flyby-solar probe missions. Only small increases in mission times result. Favorable vehicle to Earth telemetry conditions exist at perihelion passage for these missions.

Approach and flyby corridors at Venus were found to be such that, based on current guidance techniques, at least 95 percent of the minimum perihelion achievable under ideal conditions can be realized.

2. For Juipter flyby-solar probe missions with launch velocities greater than about 10.5 km/sec, solar impacts are possible for multiple flyby distances between 1 and 15 planet radii. Numerous tradeoffs exist at these minima between transfer time, telemetry conditions, launch velocity, and approach and planet perigee corridors. Superior overall mission performance was attained for a launch velocity of about 10.8 km/sec for the conditions considered in the analysis.

3. Only marginal marginal improvements over that for direct transfer orbits were achieved for Venus flyby-deep space type missions.

4. Significant increases in performance were achieved for Jupiter flyby-deep space missions. Solar system escape orbits are achievable over a wide range of approach and flyby distances for hyperbolic excess launch velocities as low as 9 km/sec.

REFERENCES

1. Ehricke, Kraft A.: Space-Flight-II Dynamics. D. Van Nostrand Company, Inc., 1962.

2. Kingsland, Louis, Jr.: Trajectory Analysis of a Grand Tour Mission to the Outer Planets. AIAA Paper No. 68-1055, AIAA 5th Annual Meeting and Technical Display, 1968.

3. Deer Wester, J. M.; and D'Haem, S. M.: Systematic Comparison of Venus Swingby Mode with Standard Mode of Mars Round Trips. AIAA Paper No. 67-27, AIAA 5th Aerospace Sciences Meeting, 1967.

4. Minovitch, M. A.: Utilizing Large Planetary Pertubations for the Design of Deep-Space, Solar-Probe, and Out-of-Ecliptic Trajectories. Technical Report No. 32-849, Jet Propulsion Laboratory, California Institute of Technology; Pasadena, California, 1965.

5. Harrison, E. F.; and McLellan, C. H.: Analysis of Use of Jupiter Gravity Turns for Tailoring Trajectories to Saturn with Consideration of Launch Opportunities. NASA TN D-3699, 1966.

6. Hamilton, T. W.: Earth-Based Navigational Capabilities for Planetary Missions. AIAA Paper No. 68-852, AIAA Guidance, Control, and Flight Dynamics Conference, 1968.

7. Kelley, H. J.; Denham, W. F.; Johnson, I. L.; and Wheatly, P. O.: An Accelerated Gradient Method for Parameter Optimization with Non-Linear Constraints. The Journal of the Astronautical Sciences, Vol. XIII, No. 4, pp. 166-169, 1966.

8. Davidson, W. C.: Variable Metric Method for Minimization. Argonne National Laboratory Report ANL-5990, 1959.

9. Fletcher, R.; and Powell, M. J. D.: A Rapidly Convergent Descent Method for Minimization. Computer Journal, July 1963.

10. Kelly, H. J.: Method of Gradients. Chapter 6 of "Optimization Techniques," G. Leitmann, Editor, Academic Press, 1962.

11. Guilfoyle, G.; Johnson, I. L.; and Wheatley, P. O.: One Dimensional Search Combining Golden Section and Cubic Fit Techniques. NASA CR-65994, 1967

APPENDIX A

SUMMARY OF EQUATIONS USED IN ANALYSES OF PLANETARY FLYBY

Equations used in the analysis are summarized below for each phase of the flyby mission. Equations unique to this analysis are derived in the Theory section of the report, while standard conic relationships used are found in reference 1.

Initial values are assumed for the variables θ_i, V_{he}, and θ_a. Values for various constants appearing in the following equations are listed in tables I and II.

Pre-Encounter Transfer Orbit from Earth

Heliocentric Departure Conditions at Earth Activity Sphere.-

$$\left.\begin{aligned}
r_i &= \left(r_{Es}^2 + \rho_E^2 - 2r_{Es}\,\rho_E \sin\theta_i\right)^{1/2} \\
\psi_i &= \sin^{-1}\left(\frac{\rho_E \cos\theta_i}{r_i}\right) \\
V_i &= \left(V_{he}^2 + U_E^2 - 2V_{he}U_E \cos\theta_i\right)^{1/2} \\
\gamma_i &= -\sin^{-1}\left(\frac{V_{he}\sin\theta_i}{V_I}\right) - \psi_i
\end{aligned}\right\} \quad \text{(A-1)}$$

Perihelion and aphelion conditions for direct transfer orbit.-

$$\left.\begin{aligned}
V_{P_d} &= \frac{\mu_s}{V_i r_i \left|\cos \gamma_i\right|} + \left[\left(\frac{\mu_s}{V_i r_i \cos \gamma_i}\right)^2 + V_i^2 - \left(\frac{2\mu_s}{r_i}\right)\right]^{1/2} \\
r_{P_d} &= \frac{V_i r_i \left|\cos \gamma_i\right|}{V_{P_d}} \\
V_{A_d} &= \frac{\mu_s}{V_{P_d} r_{P_d}} - \left[\left(\frac{\mu_s}{V_{P_d} r_{P_d}}\right)^2 + V_{P_d} - \left(\frac{2\mu_s}{r_{P_d}}\right)\right]^{1/2} \\
r_{A_d} &= \frac{V_{P_d} r_{P_d}}{V_{A_d}}
\end{aligned}\right\} \quad \text{(A-2)}$$

Conic relationship for pre-encounter ellipse.-

$$\left.\begin{aligned}
a_d &= \frac{r_{A_d} + r_{P_d}}{2} \\
b_d &= \left(r_{A_d} r_{P_d}\right)^{1/2} \\
e_d &= \frac{r_{A_d}}{a_d} - 1 \\
c_d &= a_d e_d
\end{aligned}\right\} \quad \text{(A-3)}$$

Hyperbolic Encounter at Planet

Heliocentric approach conditions at planet activity sphere.-

$$\left.\begin{aligned}
\psi_{1s} &= \sin^{-1}\left[\frac{\rho_p \sin \theta_a}{r_{ps}}\right] \\
r_{1s} &= \left[r_{ps}^2 + \rho_p^2 + 2r_{ps}\rho_p \cos\left(\theta_a + \psi_{1s}\right)\right]^{1/2} \\
V_{1s} &= \left[V_i^2 + 2\mu_s\left(\frac{1}{r_{1s}} \quad \frac{1}{r_i}\right)\right]^{1/2} \\
\gamma_{1s} &= K_2 \cos^{-1}\left[\frac{V_i r_i \cos \gamma_i}{V_{1s} r_{1s}}\right]
\end{aligned}\right\} \text{(A-4)}$$

Planet referenced approach conditions at activity sphere.-

$$\left.\begin{aligned}
V_{1p} &= \left[V_{1s}^2 + U_p^2 - 2V_{1s}U_p \cos\left(\psi_{1s} - \gamma_{1s}\right)\right]^{1/2} \\
\gamma_{1p} &= \theta_a + \psi_{1s} - \pi + \sin^{-1}\left[\frac{V_{1s} \sin\left(\psi_{1s} - \gamma_{1s}\right)}{V_{1p}}\right]
\end{aligned}\right\} \text{(A-5)}$$

Perigee conditions at planet.-

$$\left.\begin{aligned}
V_{P_f} &= \frac{\mu_p}{V_{1p}\,\rho_p\left|\cos \gamma_{1p}\right|} + \left[\left(\frac{\mu_p}{V_{1p}\,\rho_p \cos \gamma_{1p}}\right)^2 + V_{1p}^2 - \left(\frac{2\mu_p}{\rho_p}\right)\right]^{1/2} \\
r_{P_f} &= \frac{V_{1p}\,\rho_p\left|\cos \gamma_{1p}\right|}{V_{P_f}}
\end{aligned}\right\} \text{(A-6)}$$

Conic relationships for encounter orbit.-

$$\left.\begin{aligned} a_f &= \left(\frac{\mu_p}{V_{1p}^2 - \frac{2\mu_p}{\rho_p}}\right) \\ b_f &= a_f(e_f^2 - 1)^{1/2} \\ e_f &= \left(\frac{V_{p_f}^2 r_{p_f}}{\mu_p}\right) - 1 \\ c_f &= a_f e_f \end{aligned}\right\} \text{(A-7)}$$

True anomaly of encounter orbit at activity sphere.-

$$\left. n_{1f} = \frac{\frac{\pi}{2} + \gamma_{1p}}{\left|\frac{\pi}{2} + \gamma_{1p}\right|} \cos^{-1}\left[\frac{(b_f^2 - \rho_p a_f)}{\rho_p c_f}\right] \right\} \text{(A-8)}$$

Planet referenced departure conditions at activity sphere.-

$$\left.\begin{aligned} V_{2p} &= V_{1p} \\ \gamma_{2p} &= \gamma_{1p} \end{aligned}\right\} \text{(A-9)}$$

Post-Encounter Transfer Orbit

Heliocentric departure conditions at planet activity sphere.-

$$\left.\begin{aligned} r_{2s} &= \left(r_{ps}^2 + \rho_p^2 + 2r_{ps}\rho_p \cos\beta\right)^{1/2} \\ \psi_{2s} &= -\sin^{-1}\left[\frac{\rho_p \sin\beta}{r_{2s}}\right] \\ V_{2s} &= \left[V_{2p}^2 + U_p^2 + 2V_{2p}U_p \cos(\beta - \gamma_{2p})\right]^{1/2} \\ \gamma_{2s} &= -\sin^{-1}\left[\frac{V_{2p}\sin(\beta - \gamma_{2p})}{V_{2s}}\right] - \psi_{2s} \\ \beta &= \theta_a + \psi_{1s} + 2\eta_{1f} \end{aligned}\right\} \text{(A-10)}$$

Conditions on post-encounter orbit.-

$$h_{2s} = V_{2s}^2 - \frac{2\mu_s}{r_{2s}}$$

$h_{2s} <$ —— Elliptic Orbit

$h_{2s} = 0$ —— Parabolic Orbit

$h \quad >$ —— Hyperbolic Orbit

Perihelion and aphelion conditions (for elliptic orbit).-

$$\left.\begin{aligned}
V_{P_H} &= \frac{\mu_s}{V_{2s} r_{2s} \left|\cos \gamma_{2s}\right|} + \left[\left(\frac{\mu_s}{V_{2s} r_{2s} \cos \gamma_{2s}}\right)^2 + V_{2s}^2 - \frac{2\mu_s}{r_{2s}}\right]^{1/2} \\
r_{P_H} &= \frac{V_{2s} r_{2s} \left|\cos \gamma_{2s}\right|}{V_{P_H}} \\
V_{A_H} &= \frac{\mu_s}{V_{P_H} r_{P_H}} - \left[\left(\frac{\mu_s}{V_{P_H} r_{P_H}}\right)^2 + V_{P_H}^2 \quad \frac{2\mu_s}{r_{P_H}}\right]^{1/2} \\
r_{A_H} &= \frac{V_{P_H} r_{P_H}}{V_{A_H}}
\end{aligned}\right\} \text{(A-11)}$$

Conic relationships for post-encounter ellipse.-

$$\left.\begin{aligned}
a_{2H} &= \left(r_{A_H} + r_{P_H}\right)^{1/2} \\
b_{2H} &= \left(r_{A_H} r_{P_H}\right)^{1/2} \\
e_{2H} &= \frac{r_{A_H}}{a_{2H}} - 1 \\
c_{2H} &= a_{2H} e_{2H}
\end{aligned}\right\} \text{(A-12)}$$

Transfer Times and Angles

Vehicle true anomaly at insertion and encounter.-

$$\left.\begin{aligned} \eta_i &= K_1 \cos^{-1}\left[\frac{(b_d - r_i a_d)}{r_i c_d}\right] \\ \eta_{1s} &= -K_2 \cos^{-1}\left[\frac{(b_d - r_{1s} a_d)}{r_{1s} c_d}\right] \end{aligned}\right\} \text{(A-13)}$$

Vehicle eccentric anomaly at insertion and encounter.-

$$\left.\begin{aligned} E_i &= \cos^{-1}\left[\frac{(a_d - r_i)}{a_d e_d}\right] \\ E_{1s} &= \cos^{-1}\left[\frac{(a_d - r_{1s})}{a_d e_d}\right] \end{aligned}\right\} \text{(A-14)}$$

Vehicle transfer angle from insertion to encounter.-

$$\left.\alpha_{i1} = \eta_i - \eta_{1s}\right\} \text{(A-15)}$$

Vehicle transfer time from insertion to encounter.-

$$\left.t_{i1} = \pi\left(\frac{a_d^3}{\mu_s}\right)^{1/2}\left[K_1(E_i - e_d \sin E_i) + K_2(E_{1s} - e_d \sin E_{1s})\right]\right\} \text{(A-16)}$$

Earth position with respect to perihelion (r_{P_d}) at insertion and encounter.-

$$\left.\begin{aligned} \phi_{EPi} &= \eta_i - \psi_i \\ \phi_{EP1} &= \phi_{EPi} - \frac{U_E t_{i1}}{r_{ES}} \end{aligned}\right\} \text{(A-17)}$$

Planet position with respect to perihelion (r_{P_d}) at encounter and encounter.-

$$\left.\begin{aligned} \phi_{pPl} &= \eta_{1s} + \psi_{1s} \\ \phi_{pPi} &= \phi_{pPl} + \frac{U_p t_{il}}{r_{ps}} \end{aligned}\right\} \text{(A-18)}$$

Auxiliary angle and mean anomaly of hyperbolic orbit at planet.-

$$\left.\begin{aligned} H_{if} &= \cos^{-1}\left[\frac{a_f e_f}{a_f + \rho_p}\right] \\ M_{1f} &= e_p \tan H_{1f} - \ln\left[\tan\left(\frac{\pi}{4} + \frac{H_{if}}{2}\right)\right] \end{aligned}\right\} \text{(A-19)}$$

Transfer time in activity sphere of perturbing planet.-

$$\left.\left(t_f = 2M_{1f} \frac{a_f^3}{\mu_p}\right)^{1/2}\right\} \text{(A-20)}$$

Vehicle true and eccentric anomaly following encounter.-

$$\left.\begin{aligned} \eta_{2s} &= K_3 \cos^{-1}\left[\frac{(b_{2H}^2 - r_{2s} a_{2H})}{r_{2s} c_{2H}}\right] \\ E_{2s} &= K_3 \cos^{-1}\left[\frac{(a_{2H} - r_{2s})}{a_{2s} e_{2H}}\right] \end{aligned}\right\} \text{(A-21)}$$

Transfer angles from encounter to perihelion and aphelion.-

$$\left.\begin{aligned} \alpha_{2P} &= \eta_{2s} + 2\pi K_5 \\ \alpha_{2A} &= \eta_{2s} + \pi \end{aligned}\right\} \text{(A-22)}$$

Transfer times from encounter to perihelion and aphelion.-

$$\left.\begin{aligned} t_{2P} &= 2\pi \left(\frac{a_{2H}^3}{\mu_s}\right)^{1/2} \left[K_4 + (E_{2s} - e_{2H} \sin E_{2s})^{1/2}\right] \\ t_{2A} &= t_{2P} + K_5\pi \left(\frac{a_{2H}^3}{\mu_s}\right)^{1/2} \end{aligned}\right\} \text{(A-23)}$$

Transfer time from insertion to perihelion and aphelion for direct and flyby orbits.-

$$\left.\begin{aligned} t_{iP_d} &= \left(\frac{a_d^3}{\mu_s}\right)^{1/2} \left[K_5(E_i - e_d \sin E_i) + 2\pi K_6\right] \\ t_{iP_H} &= t_{i1} + t_f + t_{2P} \\ t_{iA_d} &= t_{iP_d} + \pi \left(\frac{a_d^3}{\mu_s}\right)^{1/2} (1 - 2K_6) \\ t_{iA_H} &= t_{i1} + t_f + t_{2A} \end{aligned}\right\} \text{(A-24)}$$

Earth and planet position with respect to post-encounter perihelion and aphelion.-

$$\left.\begin{aligned} \phi_{EPH} &= \phi_{EPi} + \delta\eta - \frac{U_E t_{iP_H}}{r_{Es}} \\ \phi_{EAH} &= \frac{\pi}{2} - \phi_{EPH} \\ \phi_{pPH} &= \phi_{pPi} + \delta\eta - \frac{U_p t_{iP_H}}{r_{ps}} \\ \phi_{pAH} &= \frac{\pi}{2} - \phi_{pPH} \\ \delta\eta &= \eta_{2s} - \eta_{1s} + \frac{U_p t_f}{r_{ps}} - \psi_{1s} + \psi_{2s} \end{aligned}\right\} \text{(A-25)}$$

Necessary Conditions at Insertion and Encounter

Encounter with planet inside or outside earth orbit.-

$$\left.\begin{aligned} &\text{Inside - } r_{P_d} < r_{ps} + \rho_p \\ &\text{Outside - } r_{A_d} > r_{ps} - \rho_p \end{aligned}\right\} \quad \text{(A-26)}$$

Encounter conditions.-

$$\left.\begin{aligned} &-180 < \gamma_{1p} < 0 \\ &0^{\circ} \leq \theta_a \leq 180^{\circ} \\ &V_{1s} \cos \gamma_{1s} < \frac{U_s r_{1s} \cos \psi_{1s}}{r_{ps}} \\ &180^{\circ} < \theta_a < 360^{\circ} \\ &V_{1s} \cos \gamma_{1s} > \frac{U_s r_{1s} \cos \psi_{1s}}{r_{ps}} \end{aligned}\right\} \quad \text{(A-27)}$$

APPENDIX B

DESCRIPTION OF OPTIMIZATION PROCEDURE

In the section on SURVEY OF LITERATURE various references are given which provide a detailed description of the theory associated with the numerical optimization procedure used in the present study. Thus, only an outline of the basic procedure and the practical aspects of its application will be presented.

The optimization procedure provides a method for determining the values of certain variables x which minimize some function of the variables $f(x)$ while satisfying constraints $g(x) = 0$, where x is an n-vector, f is a known scalar function of x, and g is an m-vector of known functions of x. The general form of the function to be optimized is given by

$$\bar{f} = f + \frac{1}{2} \sum_{j=1}^{m} G_j \, g_j^{\,2} \tag{B-1}$$

where the G's are weighting factors associated with the constraints and are chosen such that a proper balance is maintained between the individual contributions to $\bar{f}$ of the unconstrained function f and the constraints g_j.

Constraints may be of either an equality or inequality type. In the case of an equality constraint, the value of some parameter is required to be identically equal to a desired value. For inequality constraints, an upper and lower bound is placed on the parameter and it is allowed to assume values within these bounds. The notational form of equality and inequality constraints are as follows:

Equality $- g = (g_V - g_D)$

Inequality $- g = 0$ for (lower limit) $\leq g_V \leq$ (upper limit)

$= (g_V -$ lower limit$)$ for $g_V <$ lower limit

$=$ (upper limit $- g_V$) for $g_V >$ upper limit

where g_V is the computed value of the constrained parameter and g_D is the desired value.

It should be noted that, since the optimal value for $\bar{f}$ is achieved in an iterative fashion, violations of the constraints may occur during certain iteration cycles. However, as the optimum is approached, the constraints are forced within the required tolerances.

In addition to the unconstrained function f and the constraints g, the optimization procedure requires certain other quantities in order to establish extremum values for $\bar{f}$. These include the effects on the unconstrained function f and the constraints g_j of variations in the variables x. The sensitivity of f to changes in x is the gradient of f and is given in the form of an array

$$\nabla f = \left(\frac{\partial f}{\partial x_1}, \frac{\partial f}{\partial x_2}, \ldots, \frac{\partial f}{\partial x_n}\right) \tag{B-2}$$

The effects on the constraints of variations in the variables are supplied as an $m \times n$ matrix as follows

$$\frac{\partial g}{\partial x} = \begin{pmatrix} \frac{\partial g_1}{\partial x_1} & \frac{\partial g_1}{\partial x_2} & \cdots & \frac{\partial g_1}{\partial x_n} \\ - & - & - & - \\ - & - & - & - \\ \frac{\partial g_m}{\partial x_1} & \frac{\partial g_m}{\partial x_2} & \cdots & \frac{\partial g_m}{\partial x_n} \end{pmatrix} \tag{B-3}$$

In order to visualize the mechanization of equations (B-1) - (B-3) for a particular application, consider the following example.

Assume that we wish to establish optimal launch conditions from Earth such that minimum perihelion is achieved subject to constraints on the launch energy at Earth and the transfer angle to perihelion. While the solution for this problem can be easily established without utilizing an optimization procedure, the techniques involved are representative of those for more complicated problems.

The equations required for the assumed problem are given in appendix A by (A-1), (A-2), (A-3), and (A-17). For this problem the variables (x's) are the velocity (V_{he}) and orientation (Θ_i) of the launch trajectory. The function to be optimized (f) is the perihelion distance (r_{P_d}) associated with the launch trajectory. Constraints include the transfer angle (η_i) as well as an upper limit on launch energy (V_{he}). If we assume that the desired value for transfer angle is 120° (equality constraint), and that V_{he} can not exceed 10 km/sec (inequality constraint) then $\bar{f}$ is given by

$$\bar{f} = r_{P_d} + \frac{1}{2}\left[G_1 (\eta_i - 120^\circ)^2 + G_2 (V_{hec})^2\right] \tag{B-4}$$

where

$$V_{hec} = V_{he} - 10 \text{ for } V_{he} > 10$$

$$= 0 \qquad \text{for } V_{he} \leq 10$$

and required gradient of f and partials of the constraints are given by

$$\nabla f = \left(\frac{\partial r_{P_d}}{\partial \Theta_i}, \frac{\partial r_{P_d}}{\partial V_{he}} \right)$$

$$\frac{\partial g}{\partial x} = \begin{pmatrix} \frac{\partial \eta_i}{\partial \Theta_i}, & \frac{\partial \eta_i}{\partial V_{he}} \\ \frac{\partial V_{he}}{\partial \Theta_i}, & \frac{\partial V_{he}}{\partial V_{he}} \end{pmatrix} \tag{B-5}$$

while the partial derivatives of equations (B-5) can be determined analytically for the simple equations involved in the assumed example, for large systems of equations it is usually easier to obtain numerical partials by perturbing the variables about some nominal value.

Additional quantities require to initiate the iterative, optimization process are nominal values for the variables V_{he} and Θ_i, as well as the weighting factors on the constraints (G's). Convergence of the optimization procedure is dependent on these nominal values and weighting factors, since unrealistic values may result in computational difficulties as well as convergence to a false optimum. For example, if the G's are chosen such that the contribution to $\bar{f}$ by the constraints is negligible as compared to unconstrained function f, then the procedure will tend to ignore the constraints. Likewise, if the constraints are weighted too heavily, then the unconstrained function f will have little effect on the determination of $\bar{f}$. Poor choices of nominal values vor the variables can lead to slow convergence to the optimum resulting in increased computational time.

ACKNOWLEDGMENTS

The author expresses appreciation to Dr. A. Keith Furr, his Thesis advisor. The encouragement, patience, and technical assistance provided by Dr. Furr were invaluable in the formulation and execution of the study reported in this thesis.

VITA

The author was born on [redacted] He completed his public schooling at Emory, Virginia in 1951. He obtained a Bachelor of Science degree in Physics at Emory and Henry College in 1955. He attended graduate school at the University of Virginia during 1955-1956 serving as a graduate assistant in Physics.

The author has been employed at Langley Research Center, National Aeronautics and Space Administration from 1957 to the present date. In 1964, he attended Virginia Polytechnic Institute to complete the course requirements for a Master of Science degree in Physics.

TABLE I.- PHYSICAL CONSTANTS

	Sun	Venus	Jupiter	Earth
μ, km^3/sec^2	1.32495×10^{11}	3.2423×10^5	1.265×10^8	3.9858×10^5
U, km/sec	--	35.003	13.051	29.77
ρ, km	--	6.1594×10^5	4.8079×10^7	9.2391×10^5
Distance to sun, km	--	1.0814×10^8	7.7782×10^8	1.495×10^8

TABLE II.- CONSTANTS USED IN EQUATIONS OF APPENDIX A

FOR DETERMINING TRANSFER ANGLES AND TIMES

Pre-Encounter Transfer Condition	Post-Encounter Transfer Condition	K_1	K_2	K_3	K_4	K_5	K_6
Inside Earth orbit ($\theta_i = 0$)		1	-1			1	0
Outside Earth orbit ($\theta_i = 180^\circ$)		-1	1			-1	1
	Pre-Perihelion ($-\gamma_{2s}$)			1	0		
	Pre-Aphelion ($+\gamma_{2s}$)			-1	1		

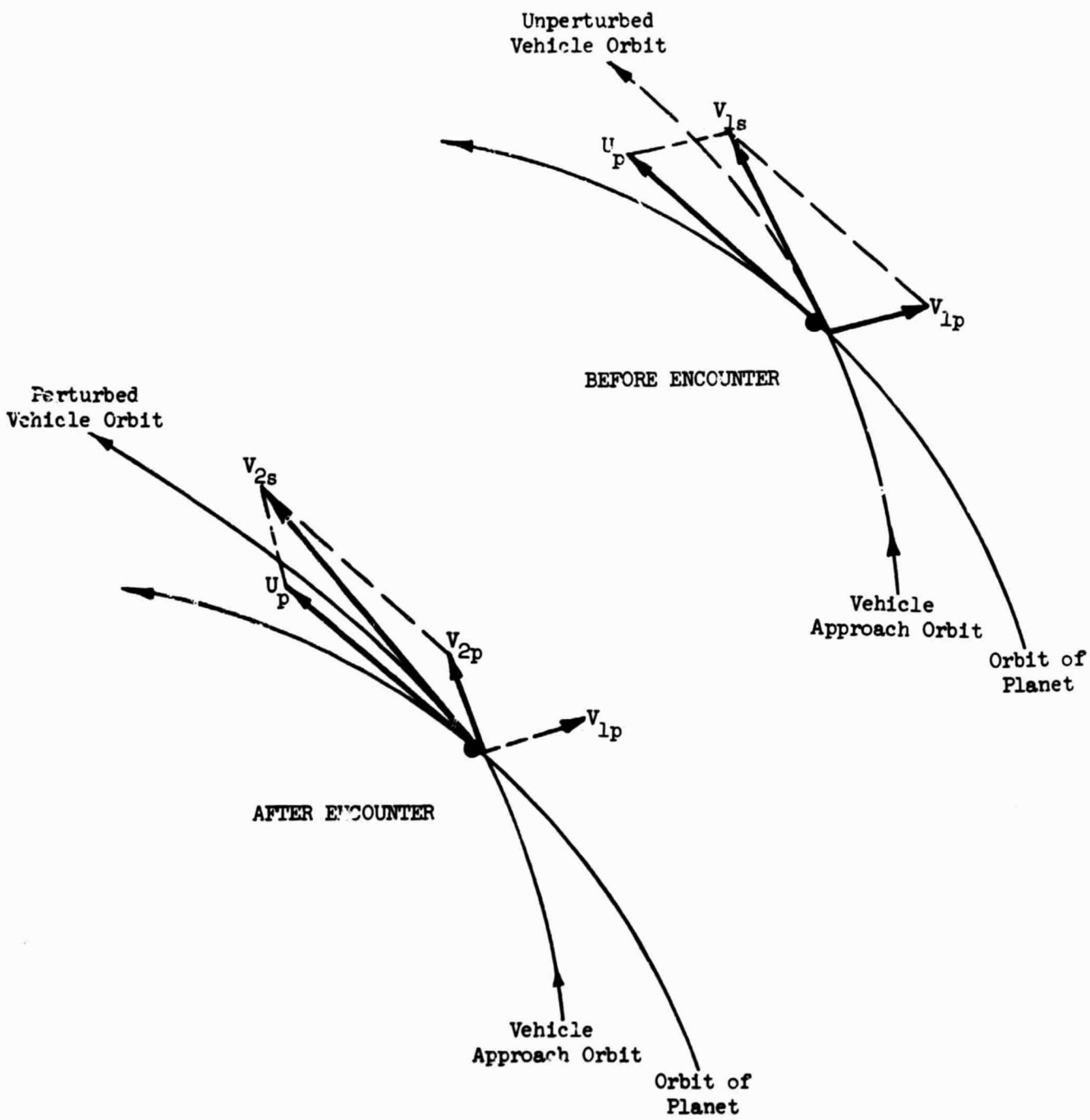

Figure 1.- Illustration of encounter involving increase in vehicle velocity.

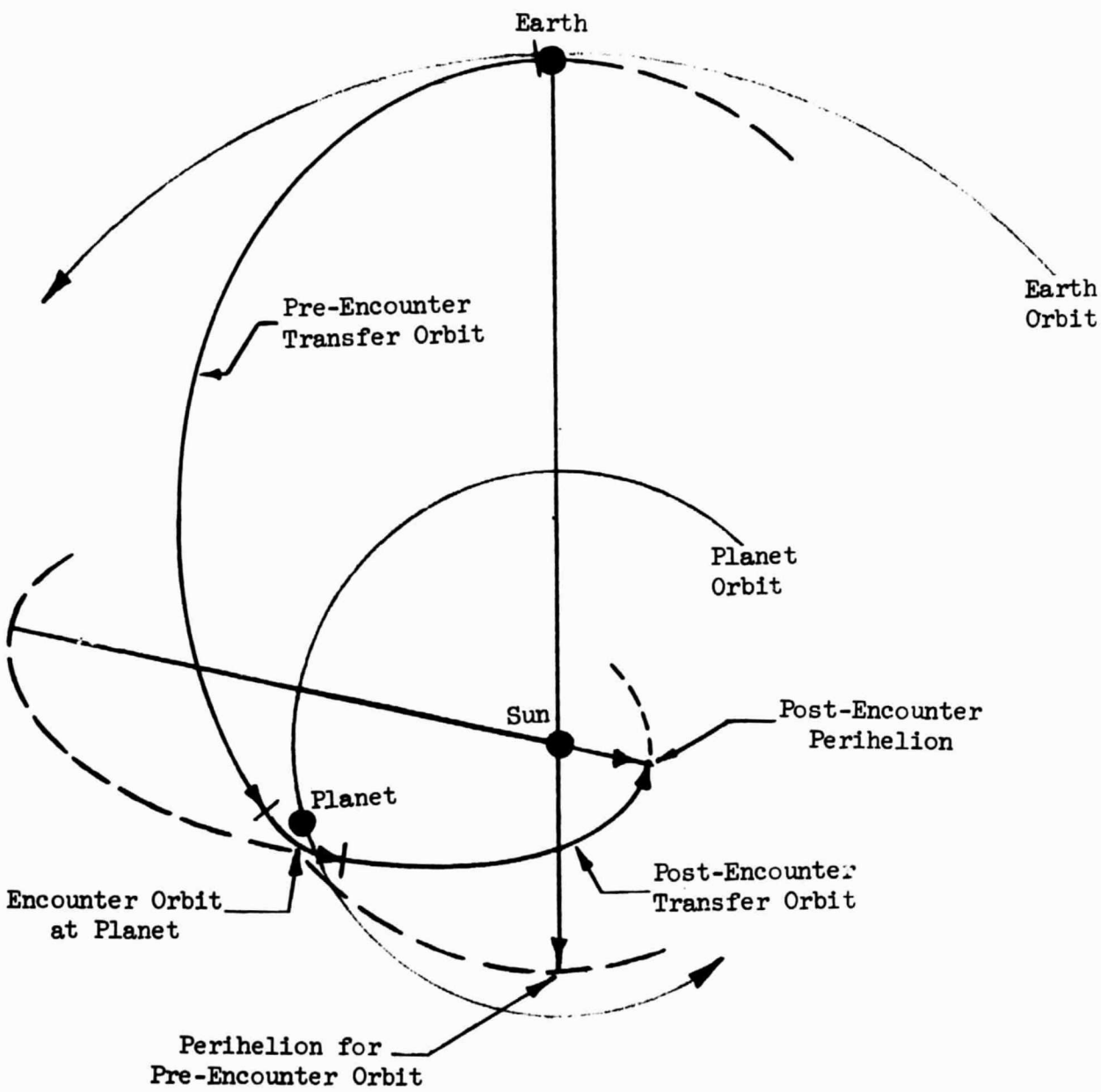

Figure 2.- Illustration of various phases of typical flyby mission.

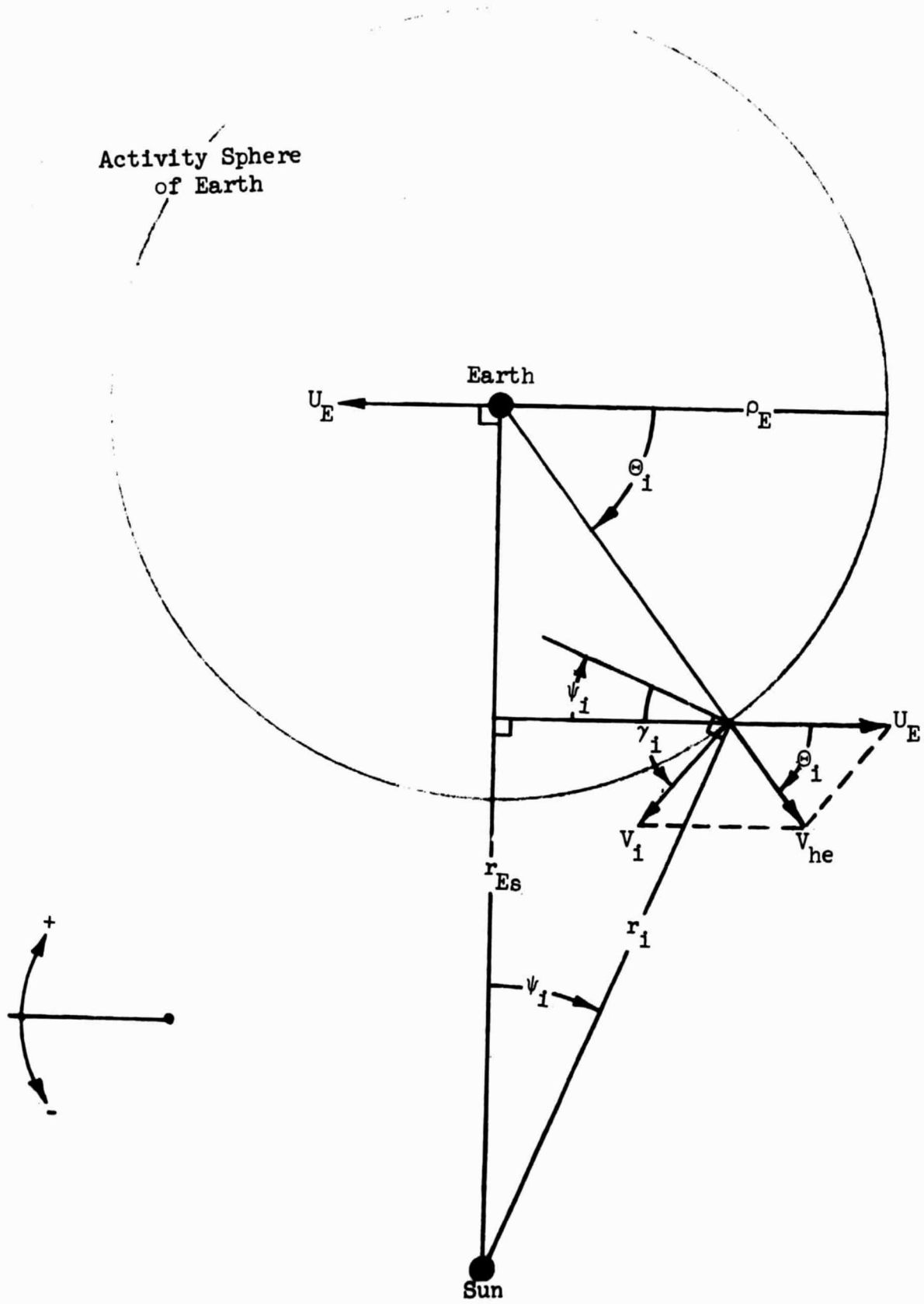

Figure 3.- Geometry used to initiate pre-encounter orbit at Earth.

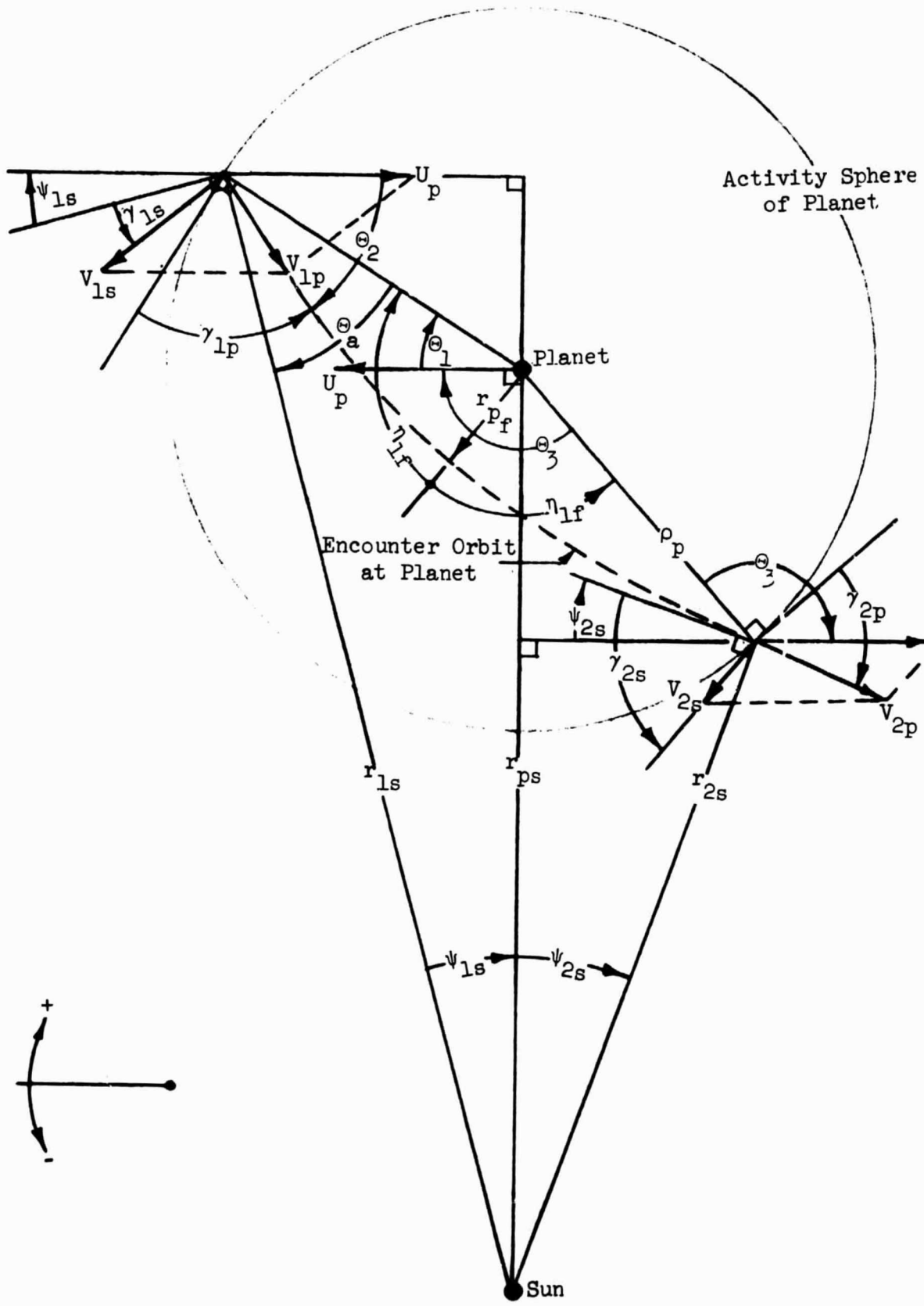

Figure 4.- Geometry of hyperbolic encounter at planet.

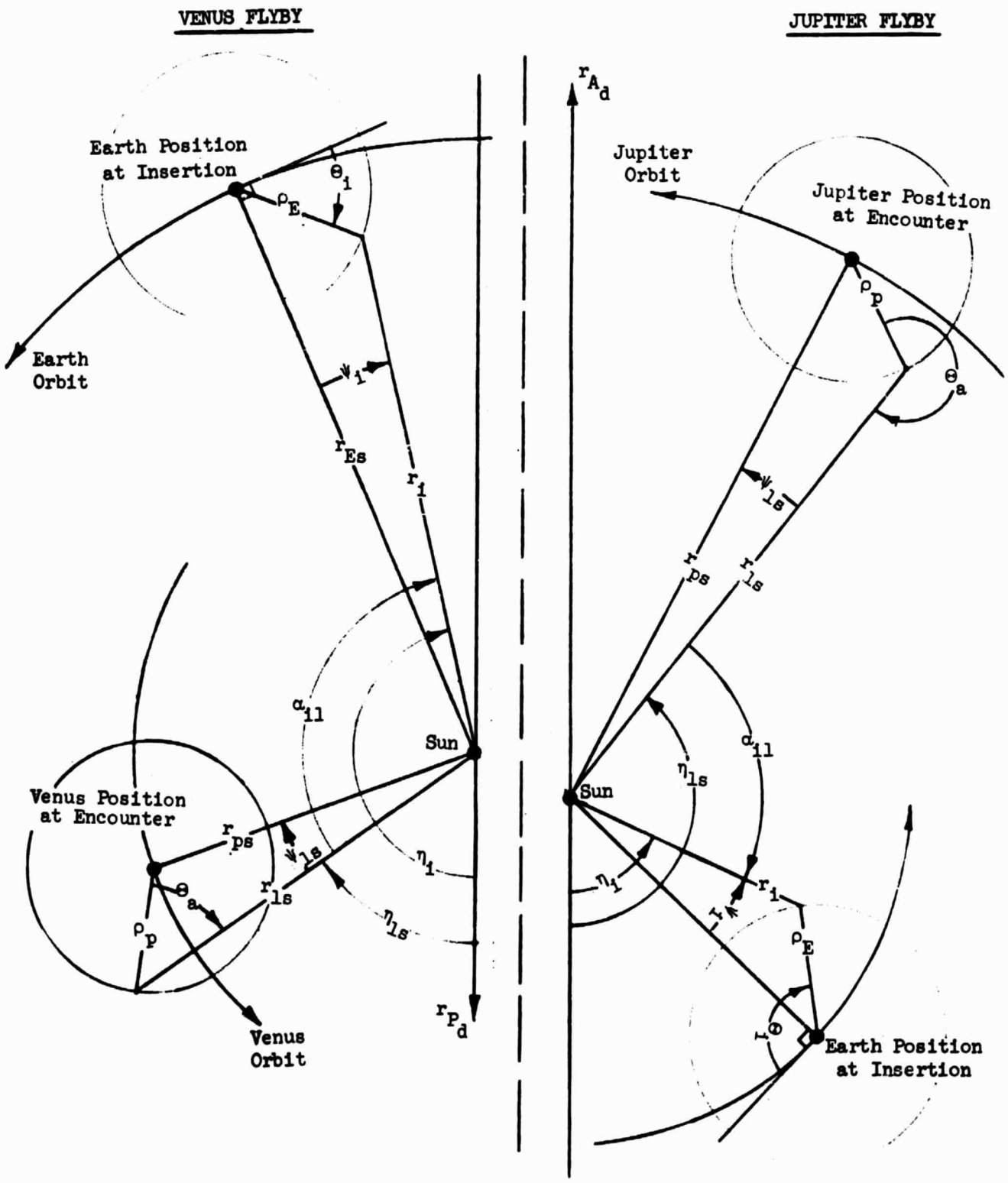

Figure 5.- Geometry used to establish transfer angles and times.

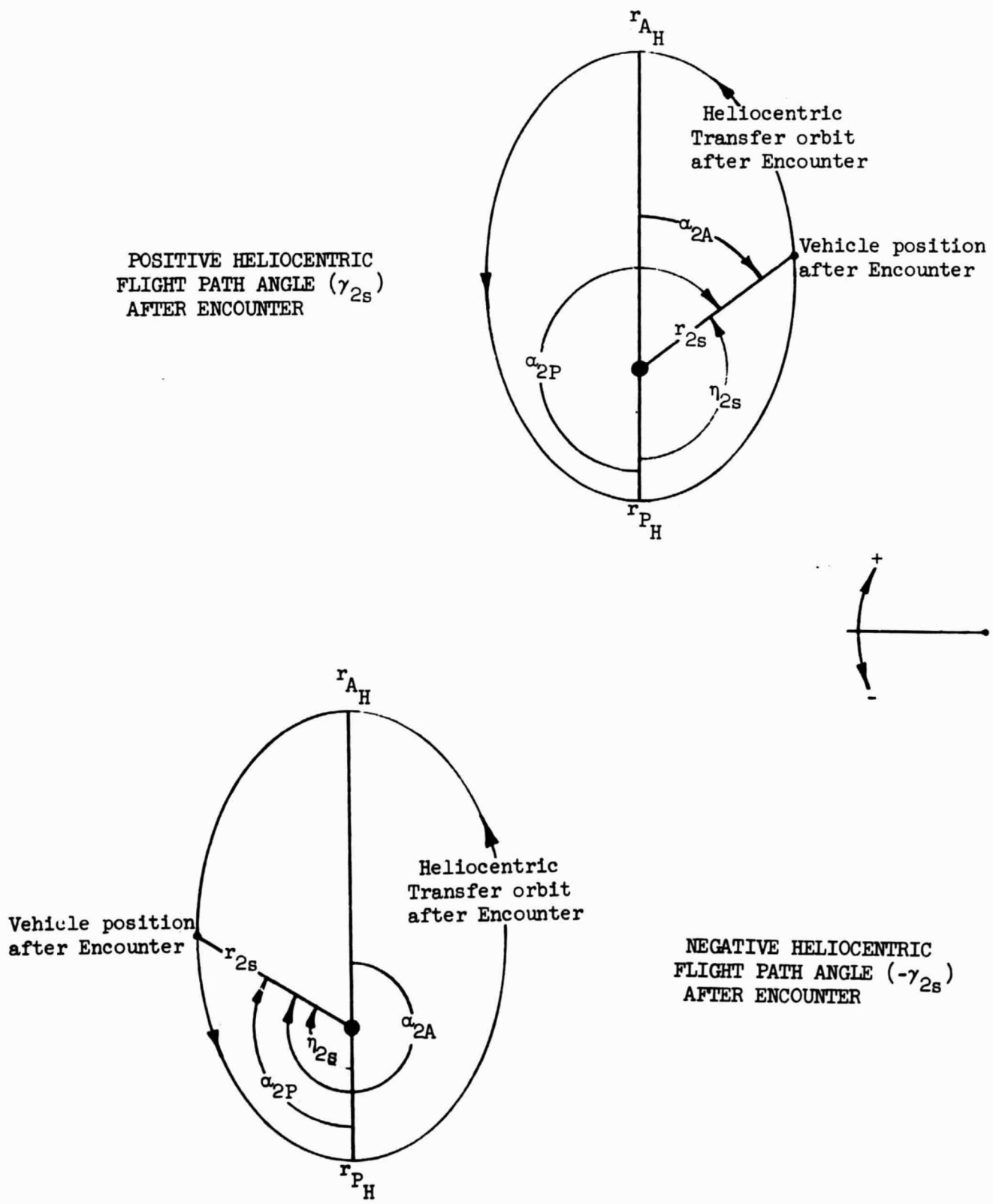

Figure 6.- Geometry used to establish transfer times and angles for post-encounter phase of mission.

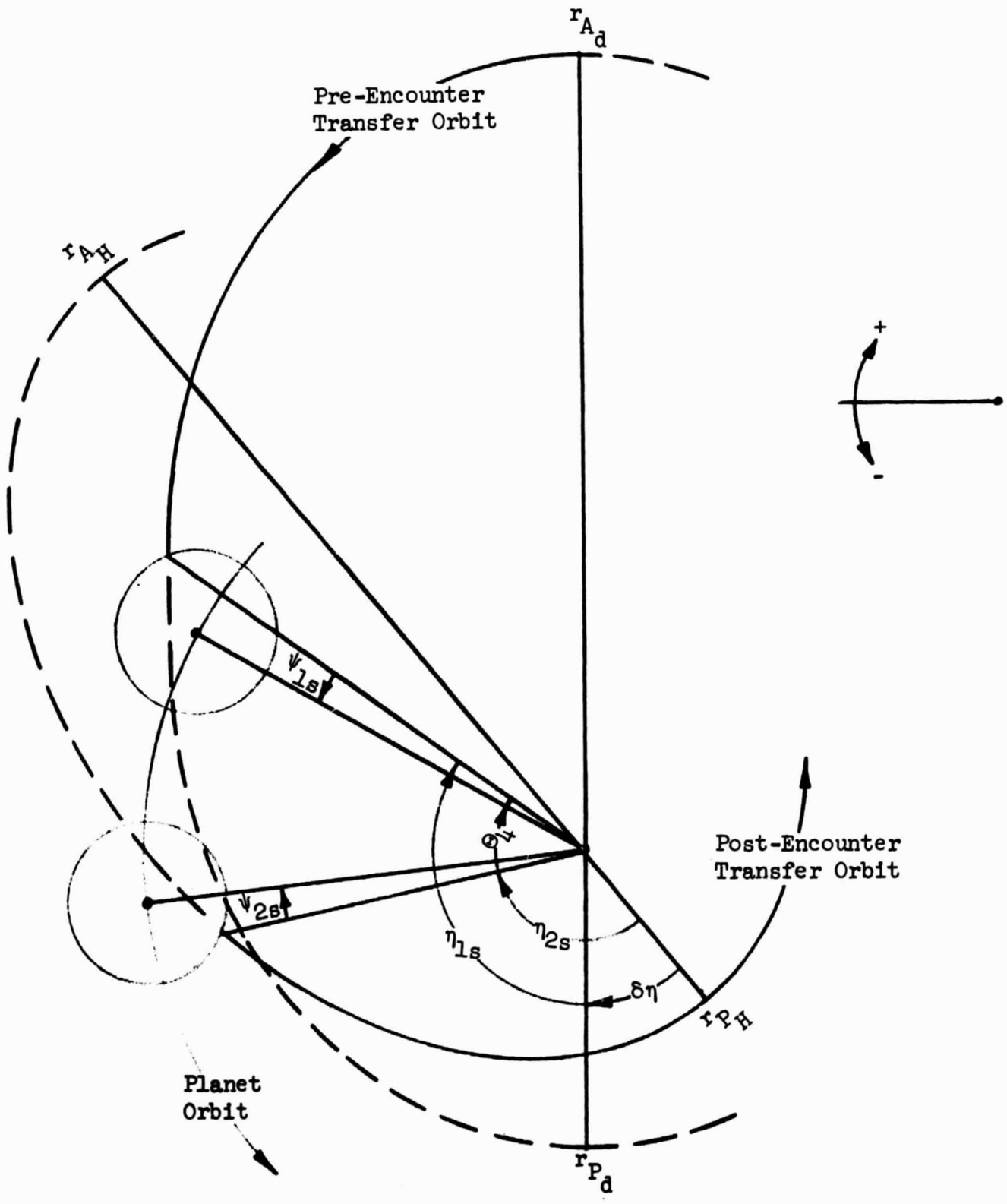

Figure 7.- Geometry used to establish Earth and planet position with respect to post-encounter aphelion and perihelion.

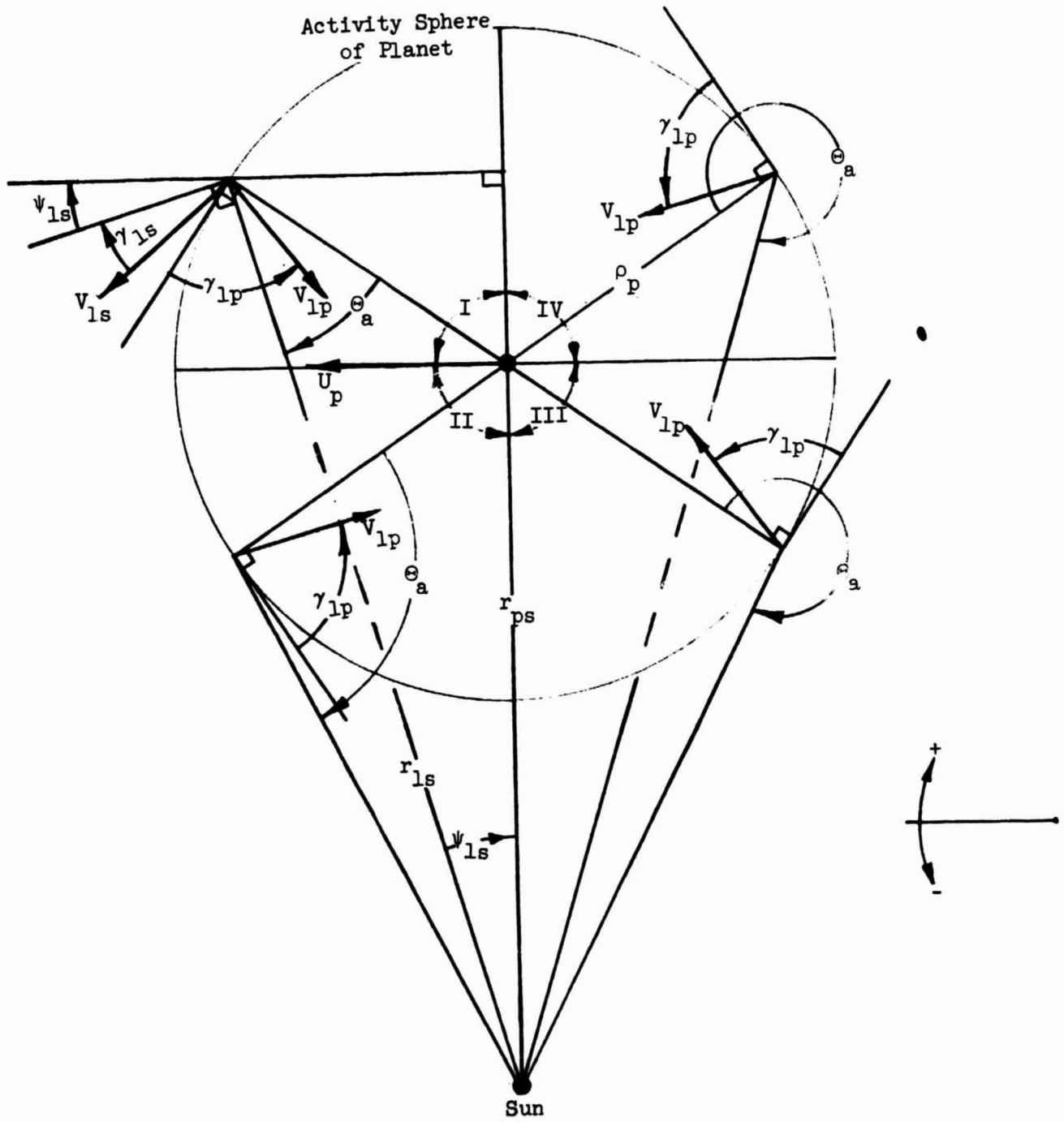

Figure 8.- Geometry used to define necessary conditions for encounter and for showing how the approach conditions determine if encounter is retrograde or direct.

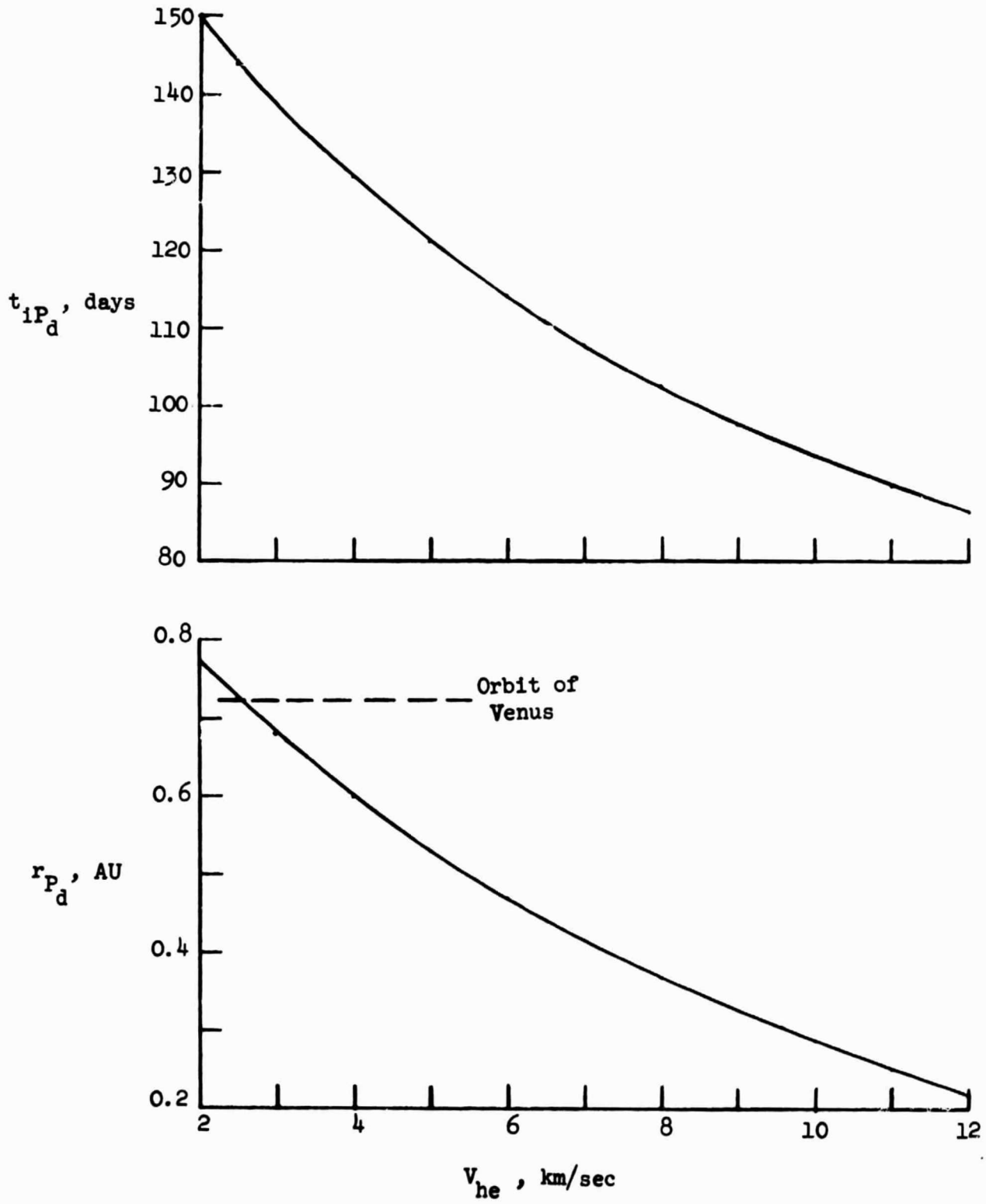

(a) Perihelion distance and transfer time from insertion to perihelion for various launch velocities ($\theta_i = 0$).

Figure 9.- Characteristics of direct transfer orbits.

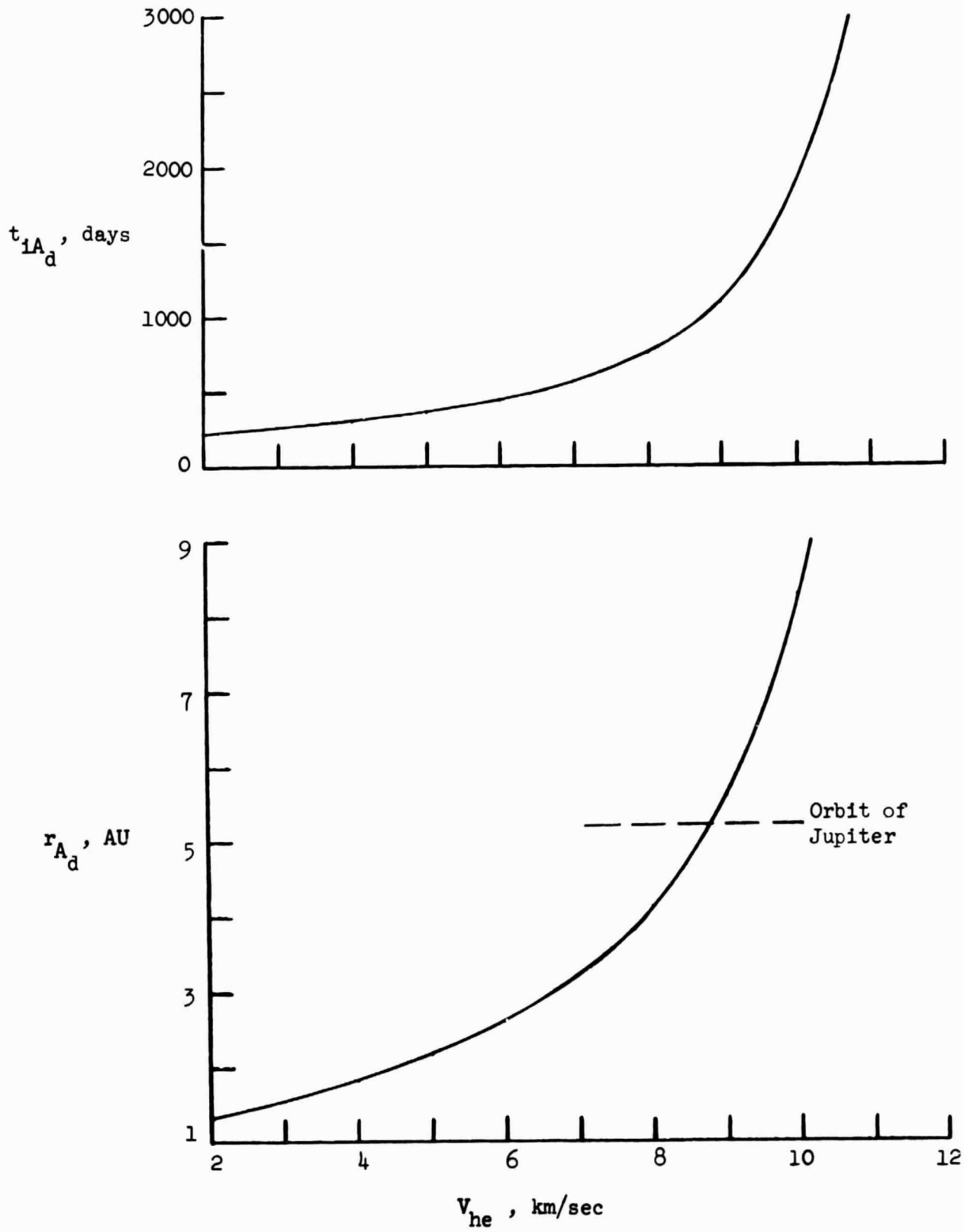

(b) Aphelion distance and transfer time from insertion to aphelion for various launch velocities (Θ_i = 180).

Figure 9.- Concluded.

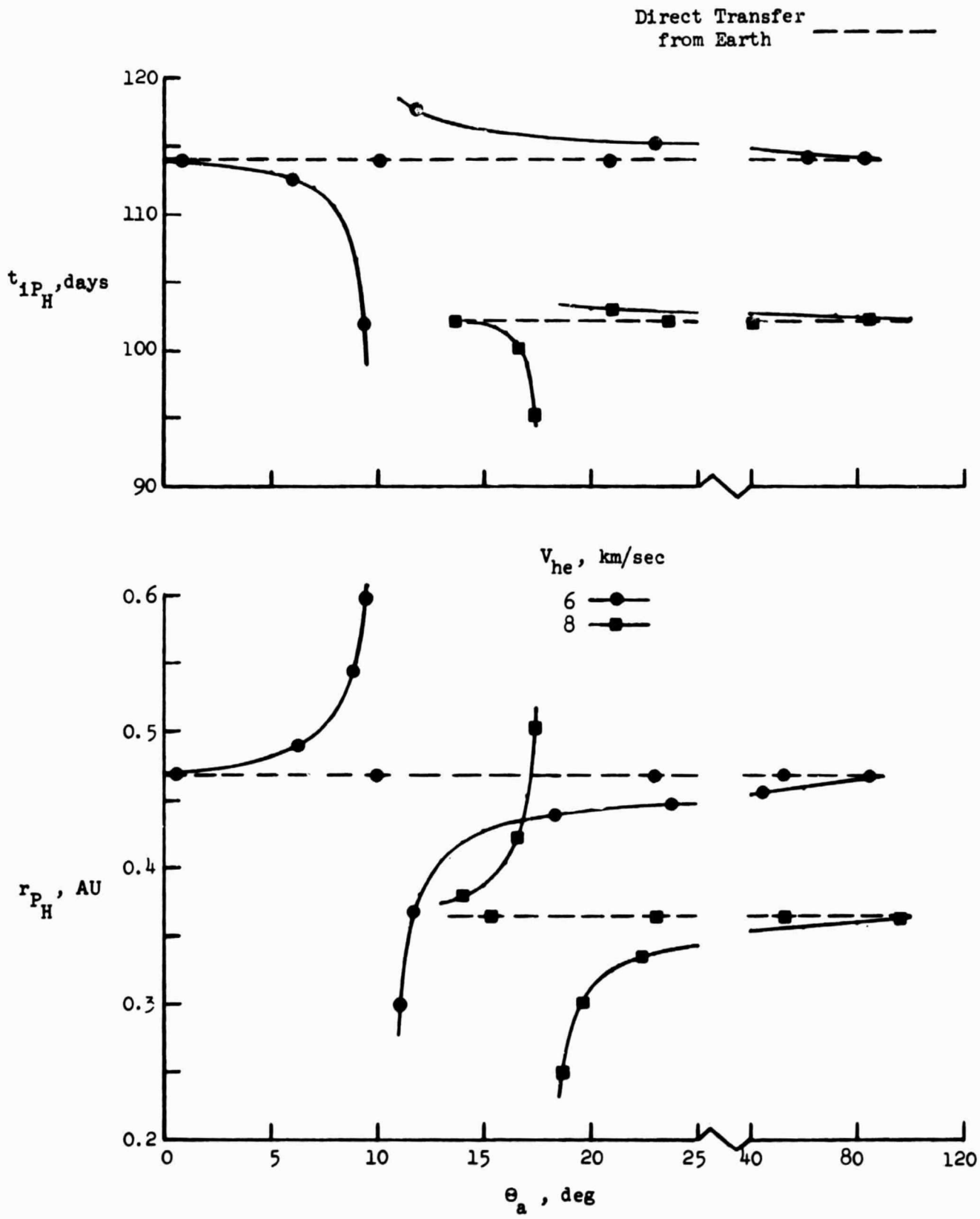

Figure 10.- Post-encounter perihelion and transfer time from insertion to perihelion for various launch velocities and planetary approach conditions at Venus.

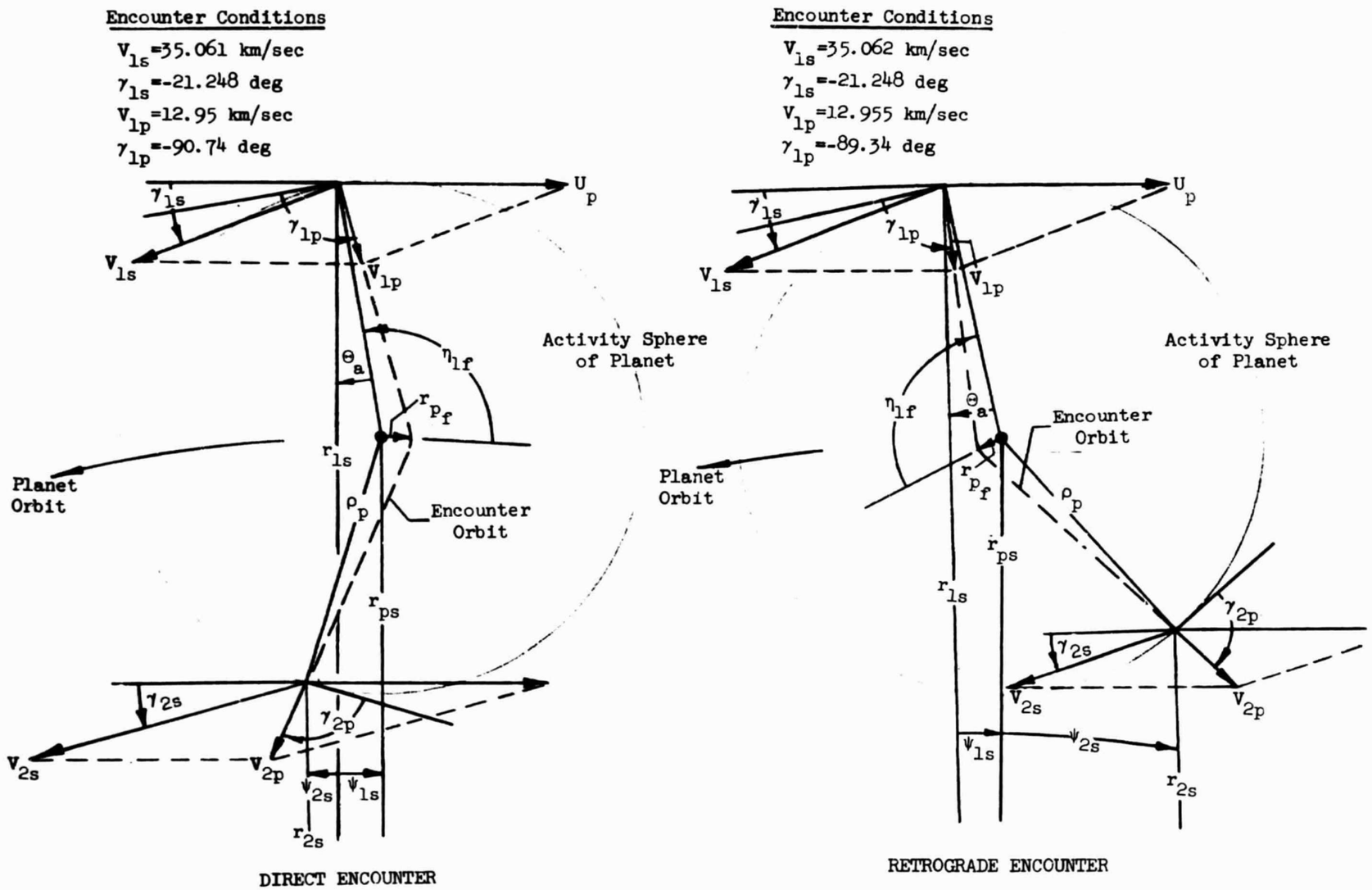

Figure 11.- Flyby orbits at Venus for direct and retrograde encounters.

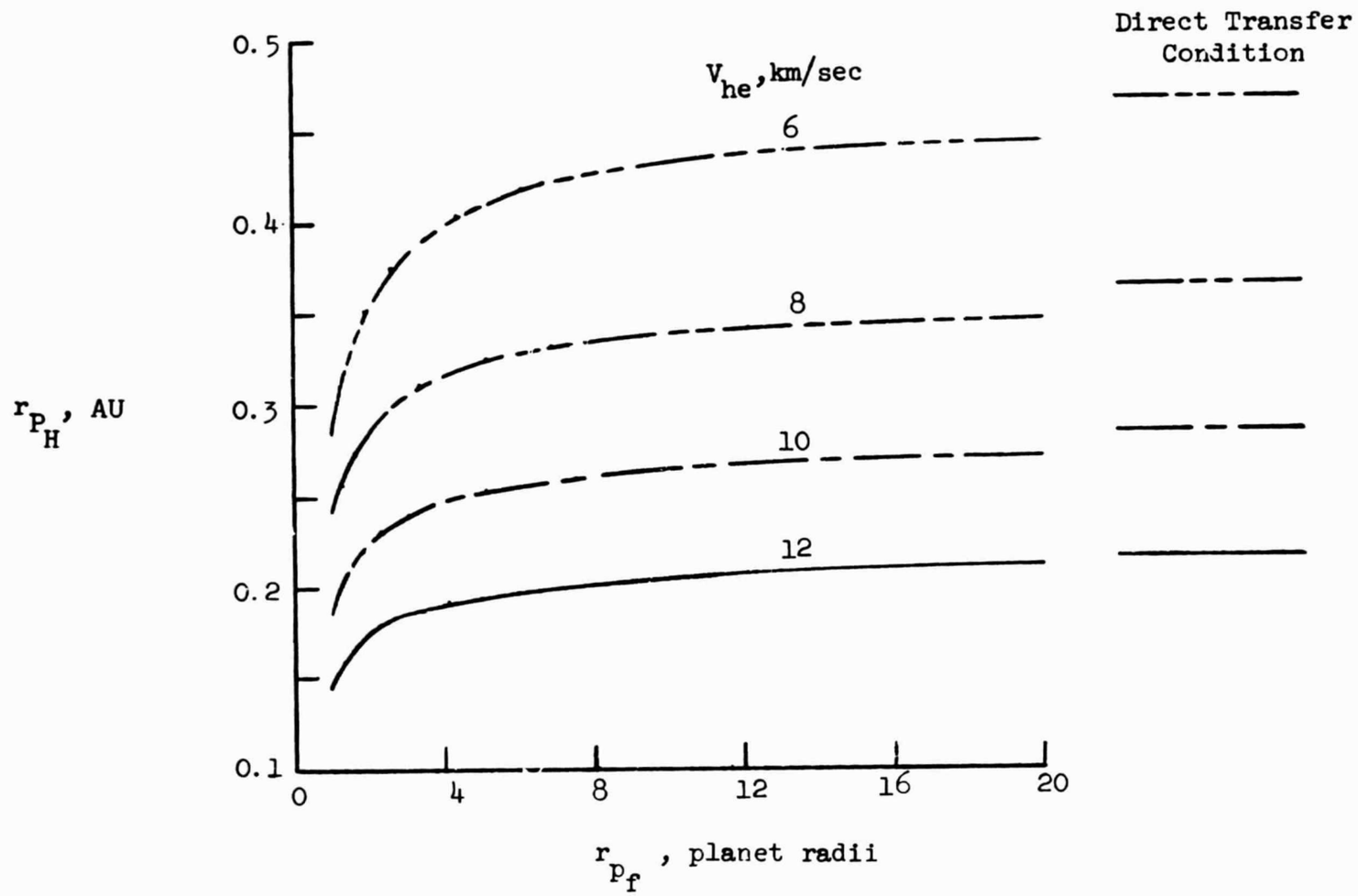

Figure 12.- Post-encounter perihelion attainable for various launch velocities and flyby distances at Venus.

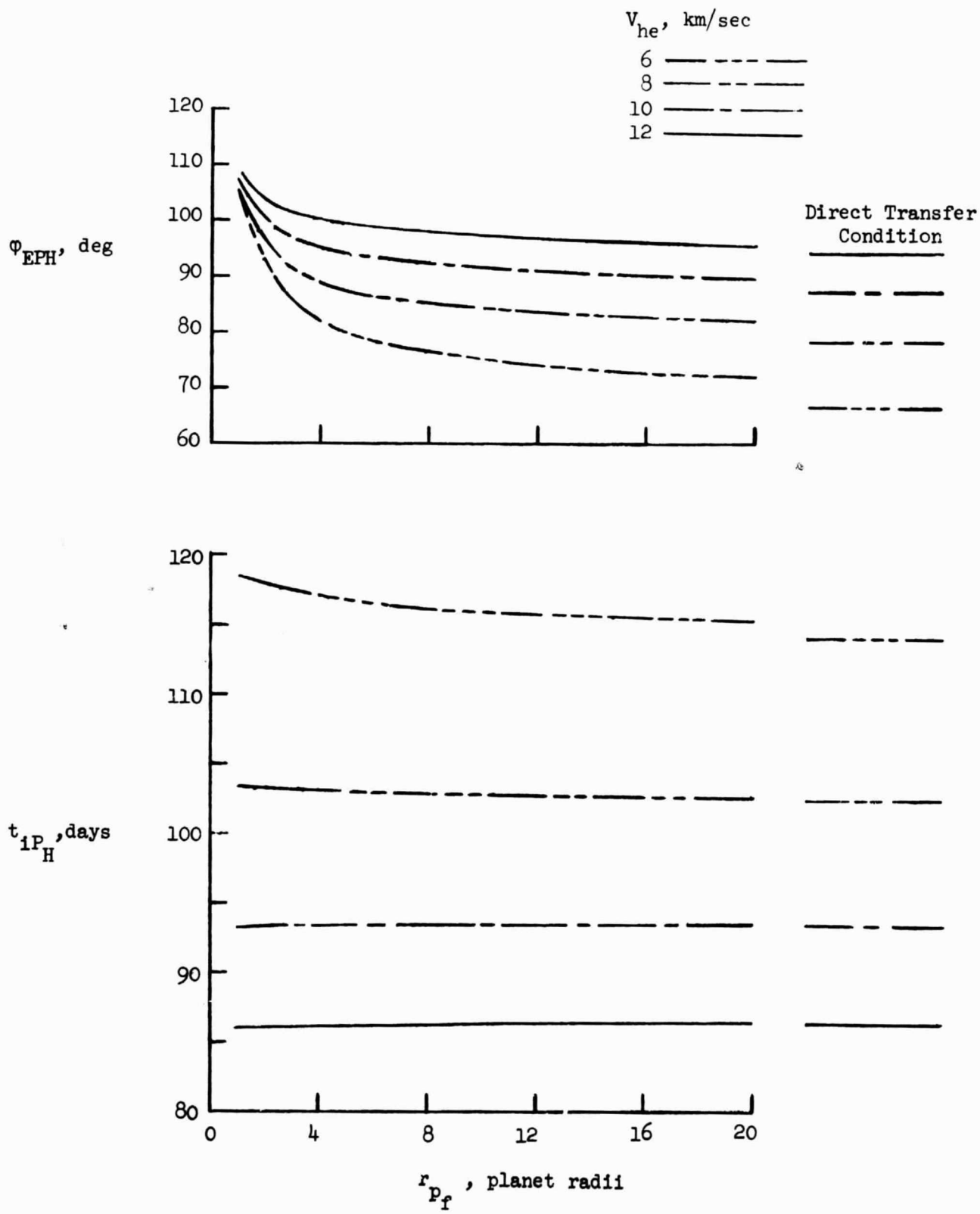

Figure 13.- Mission time and Earth position with respect to post-encounter perihelion for various launch velocities and flyby distances at Venus.

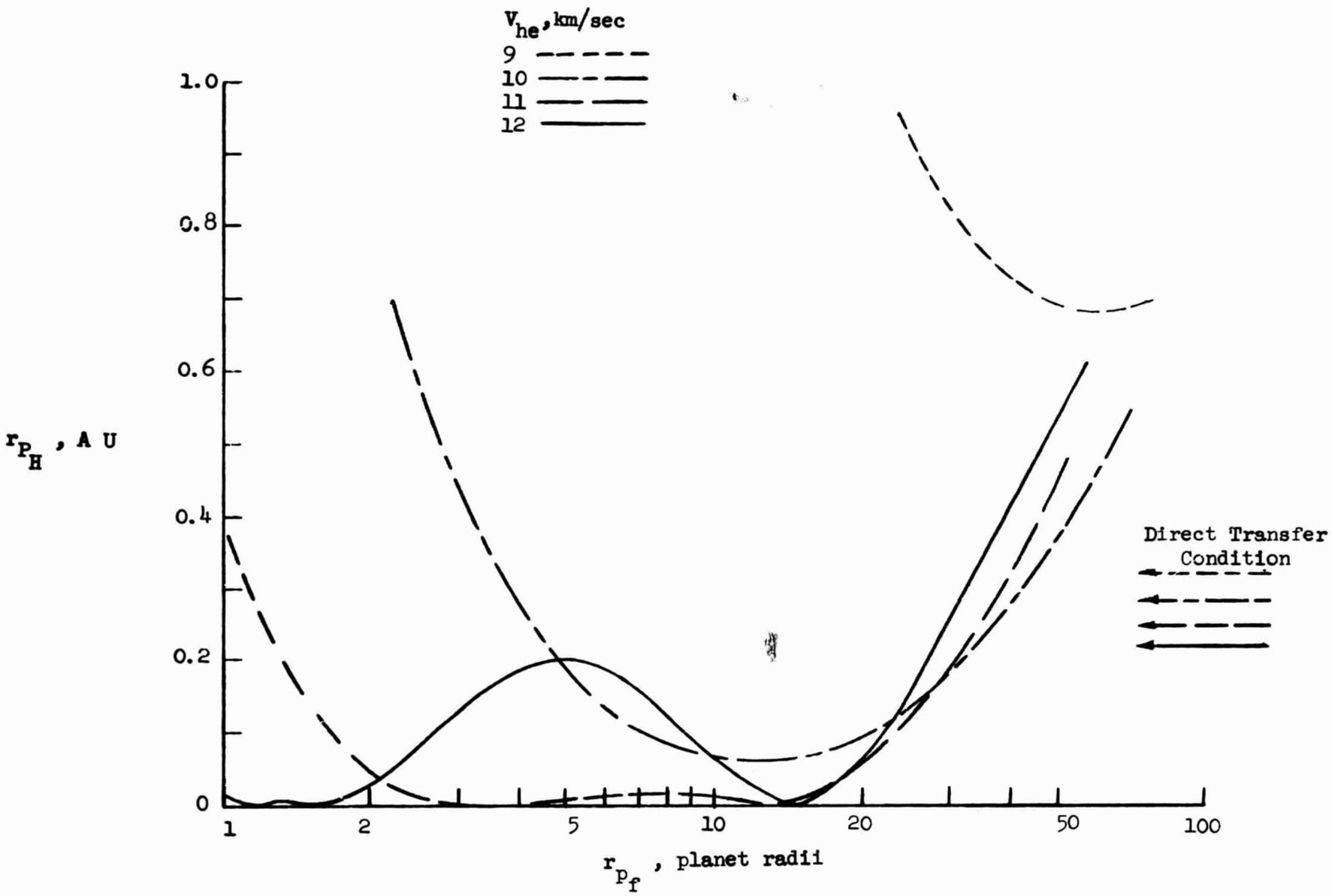

Figure 14.- Post-encounter perihelion attainable for various launch velocities and flyby distances at Jupiter.

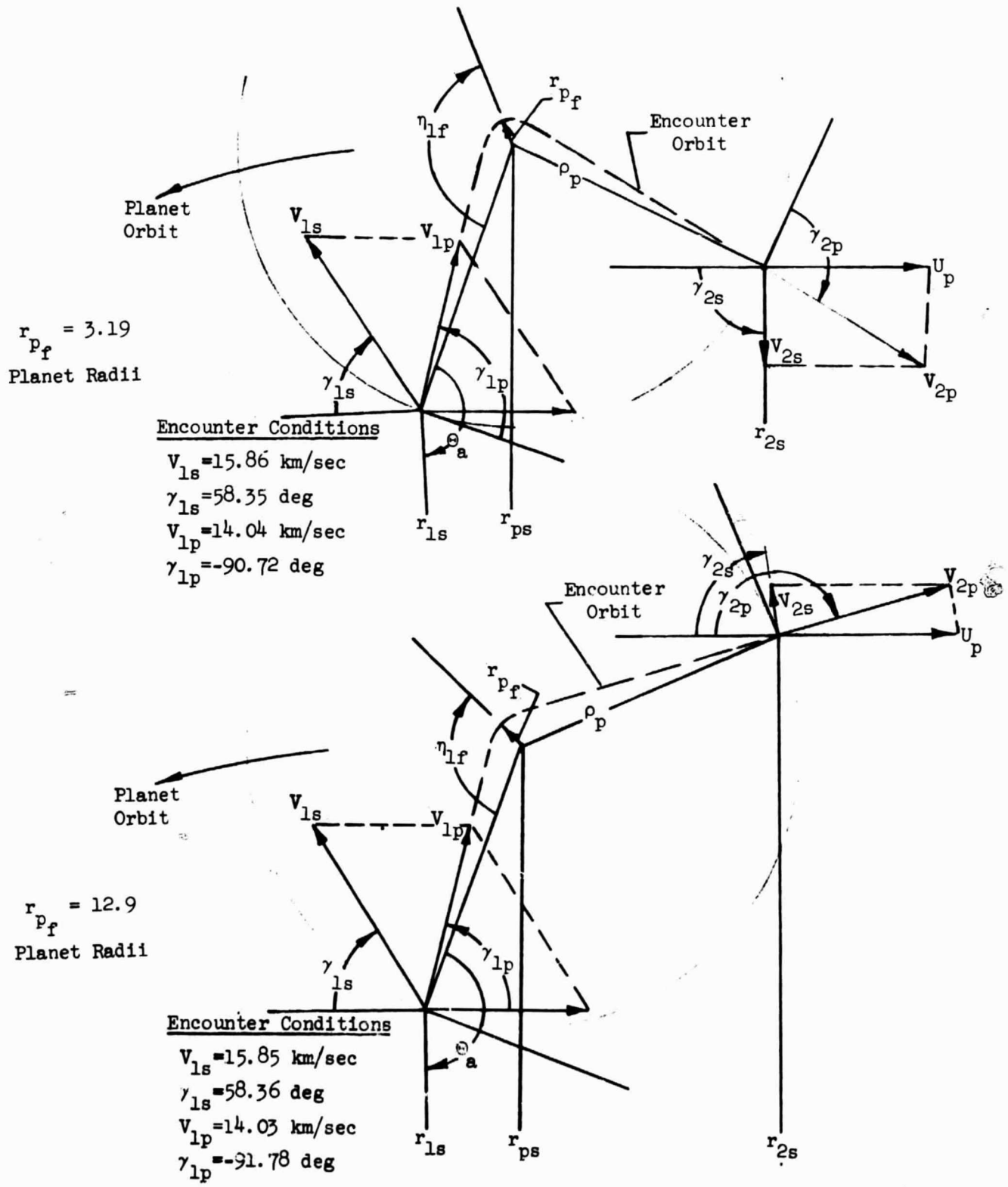

Figure 15.- Encounter orbits at Jupiter for different values of flyby distance.

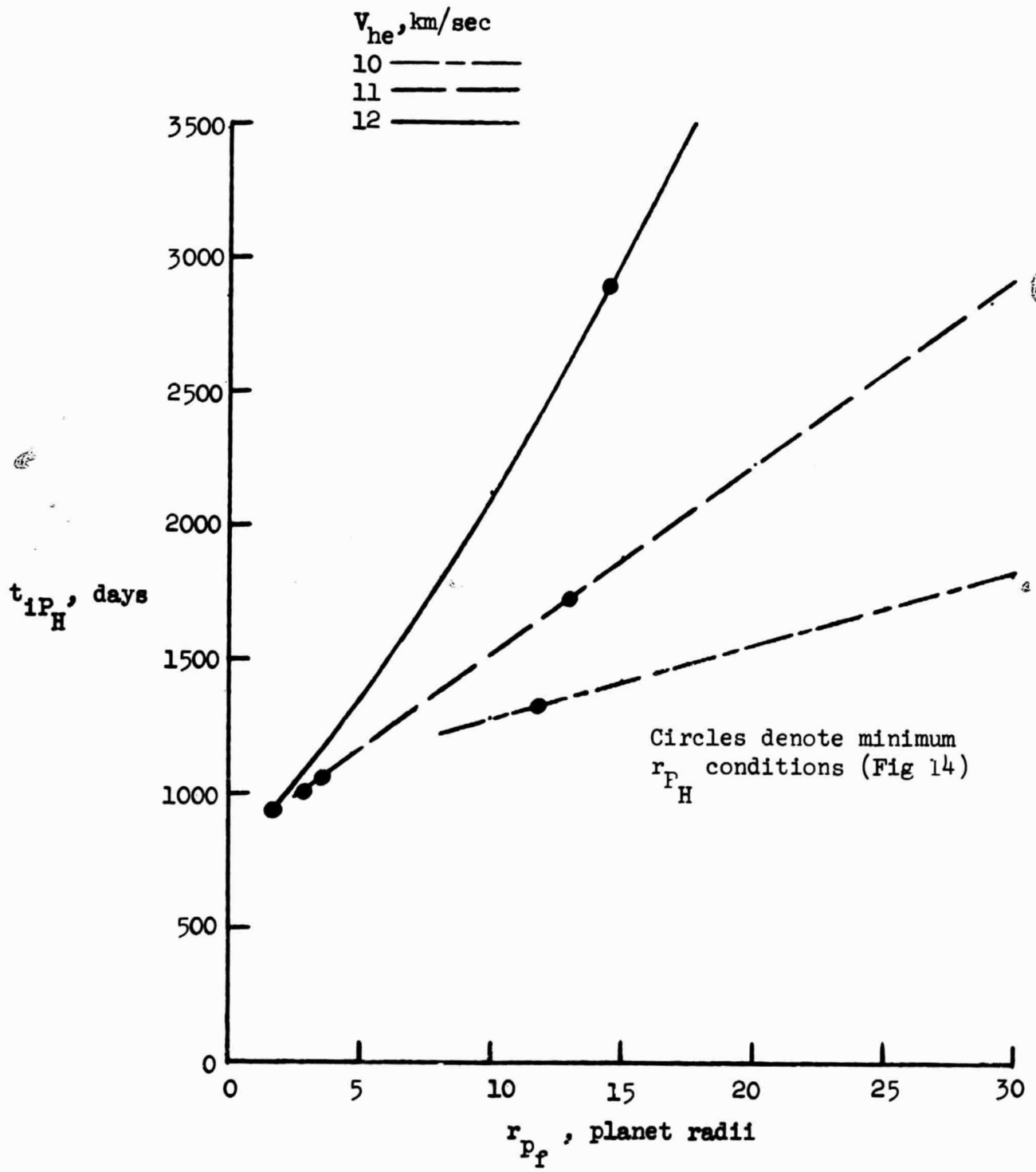

Figure 16.- Transfer time from insertion to perihelion for various launch velocities and flyby distances at Jupiter.

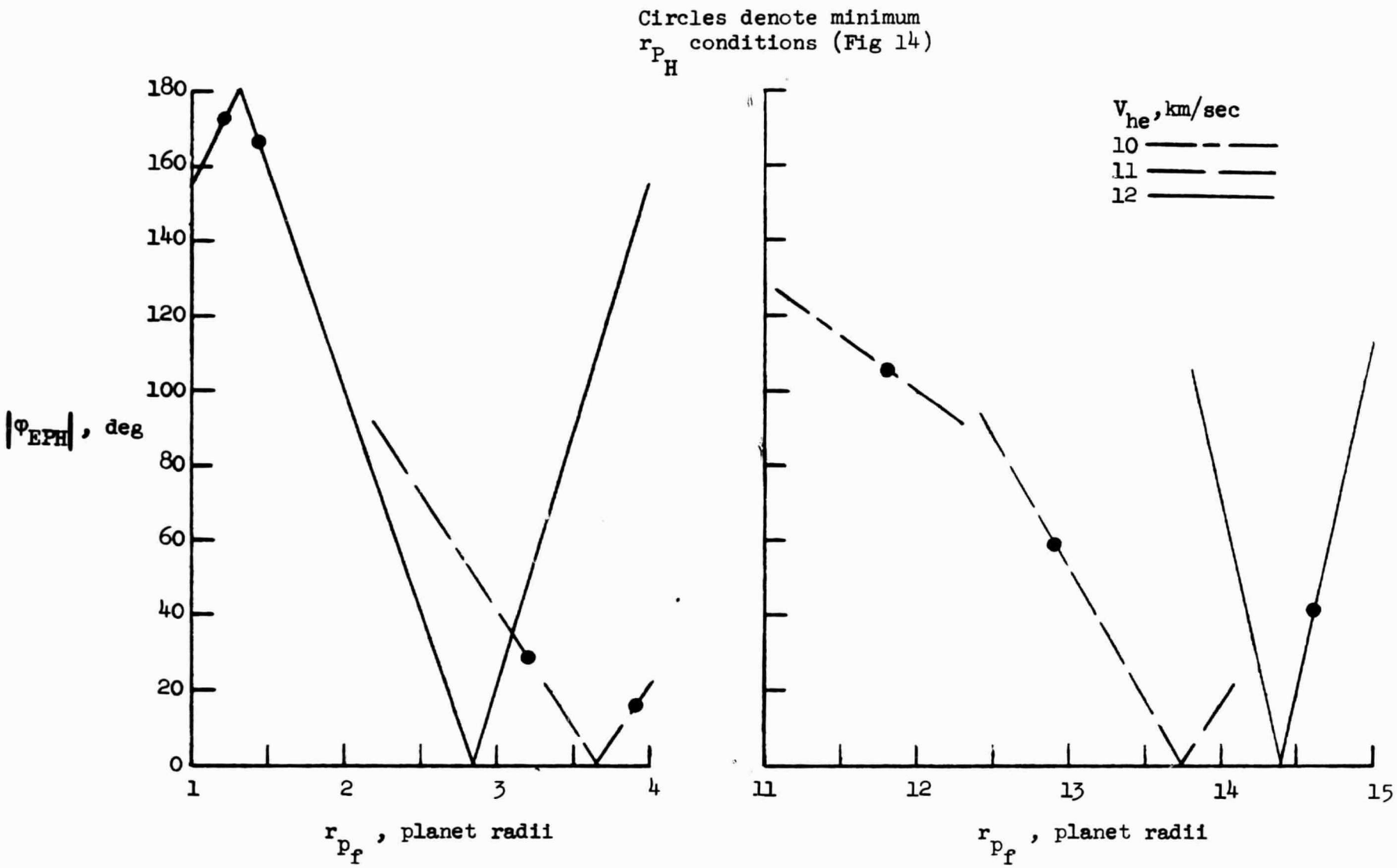

Figure 17.- Earth position with respect to post-encounter perihelion for various launch velocities and flyby distances at Jupiter.

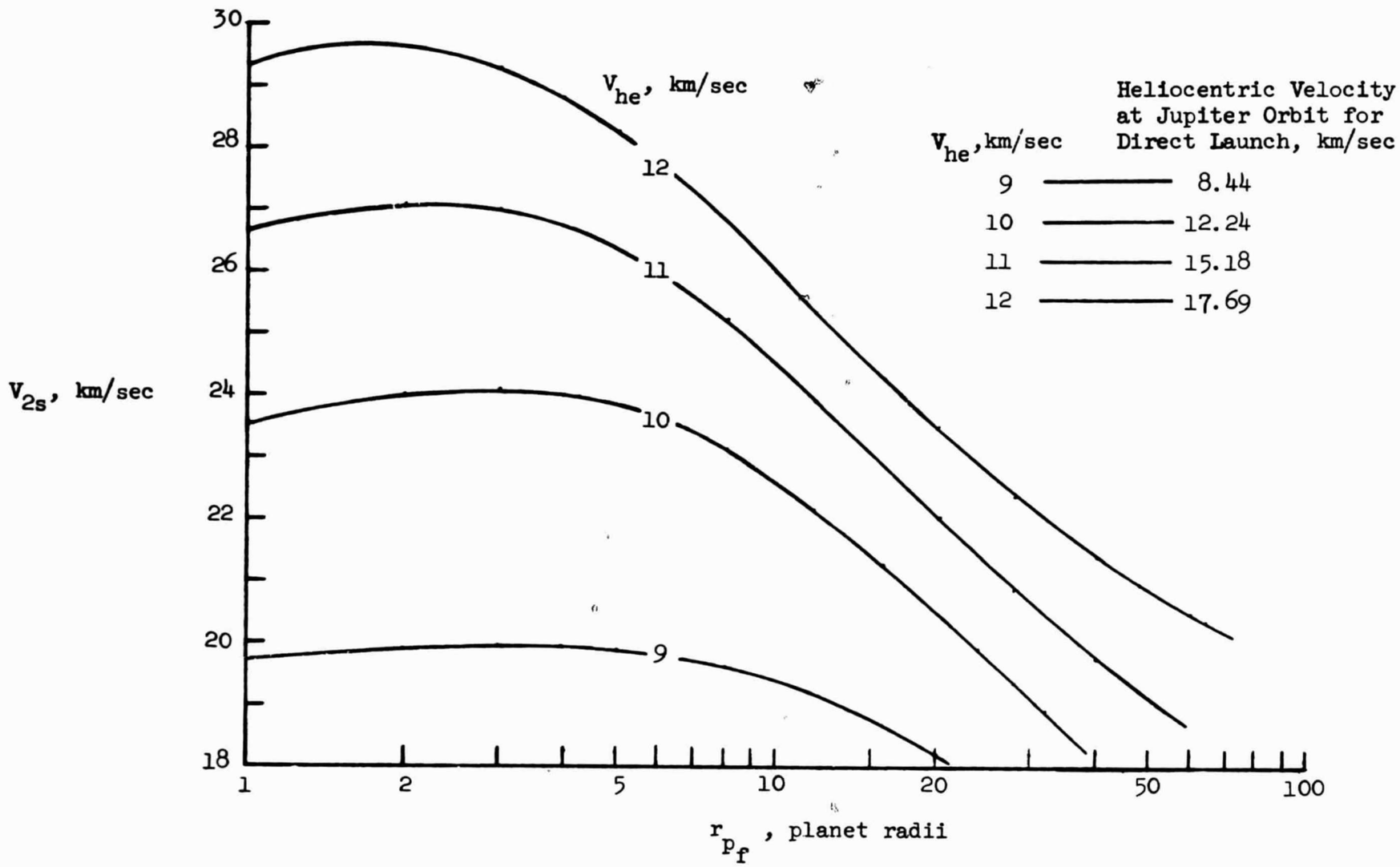

Figure 18.- Maximum heliocentric velocity attainable via flyby at Jupiter at various distances of closest approach.

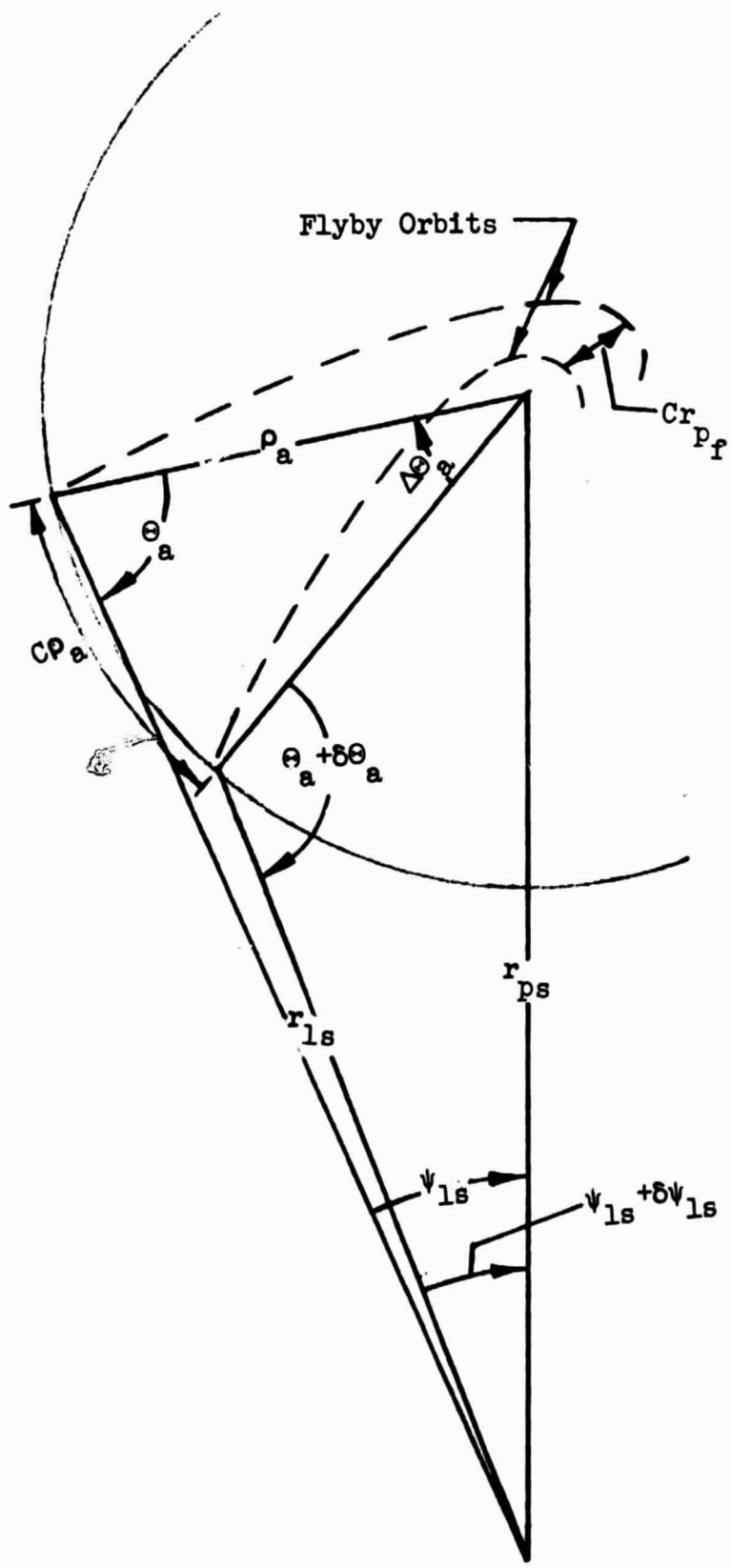

Figure 19.- Geometry used to establish approach corridor at planet activity sphere and corridor at perigee.

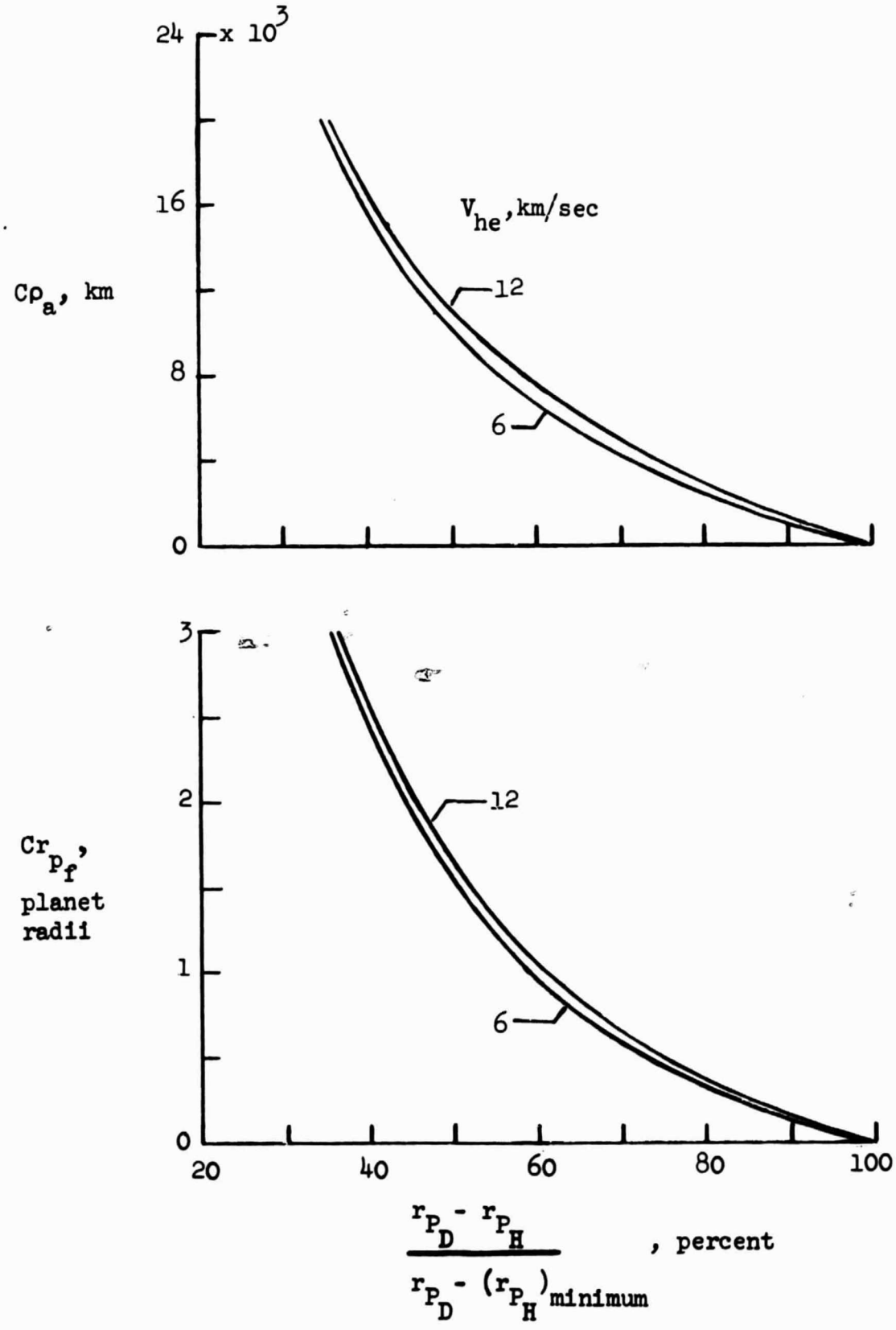

Figure 20.- Variation in approach and perigee corridors with percent of minimum perihelion achieved for Venus flyby-solar probe missions.

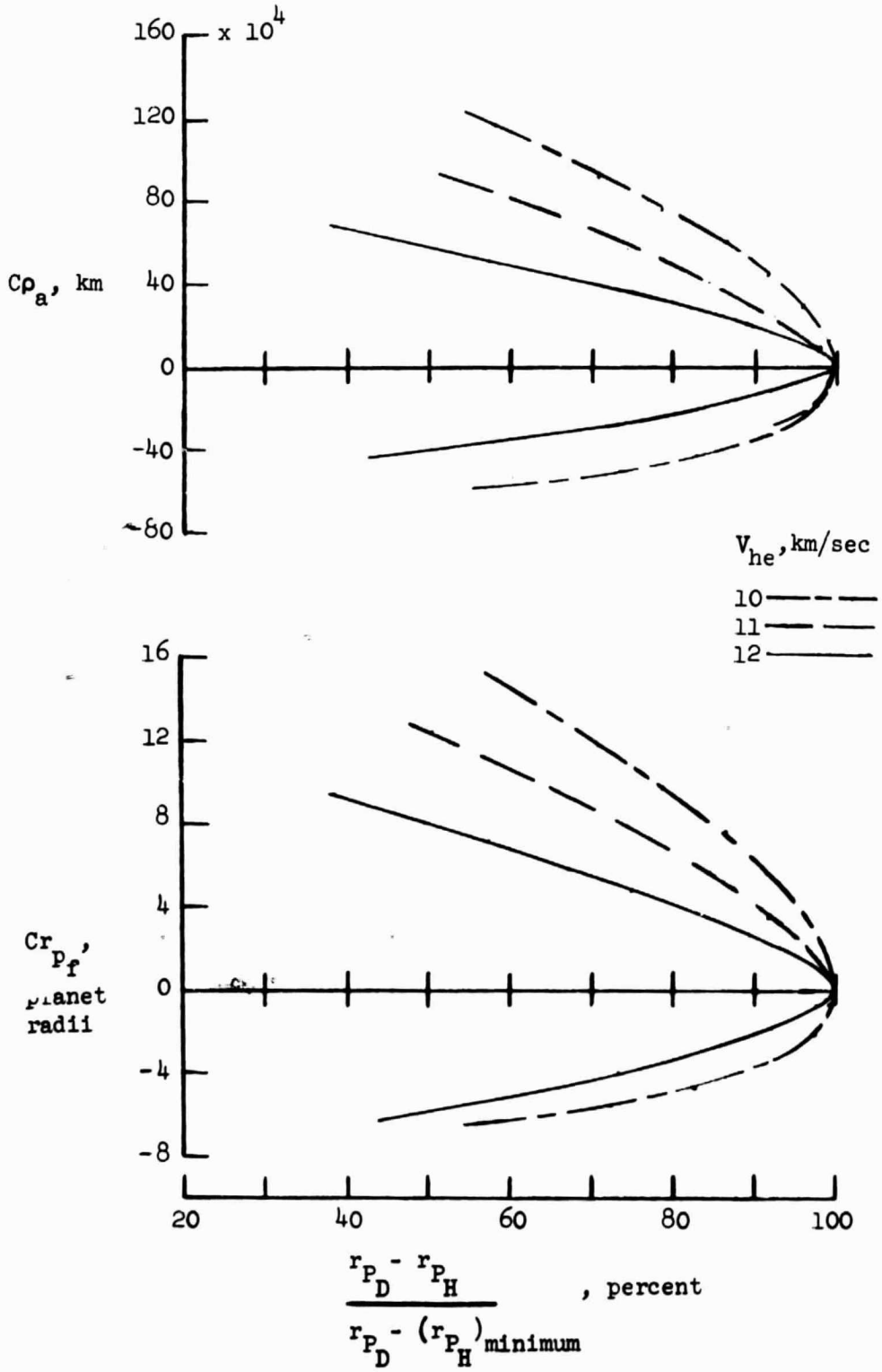

(a) Corridors for flyby distance greater than 6 planetary radii (fig. 14).

Figure 21.- Variation in approach and perigee corridors with percent of minimum perihelion achieved for Jupiter flyby-solar probe missions.

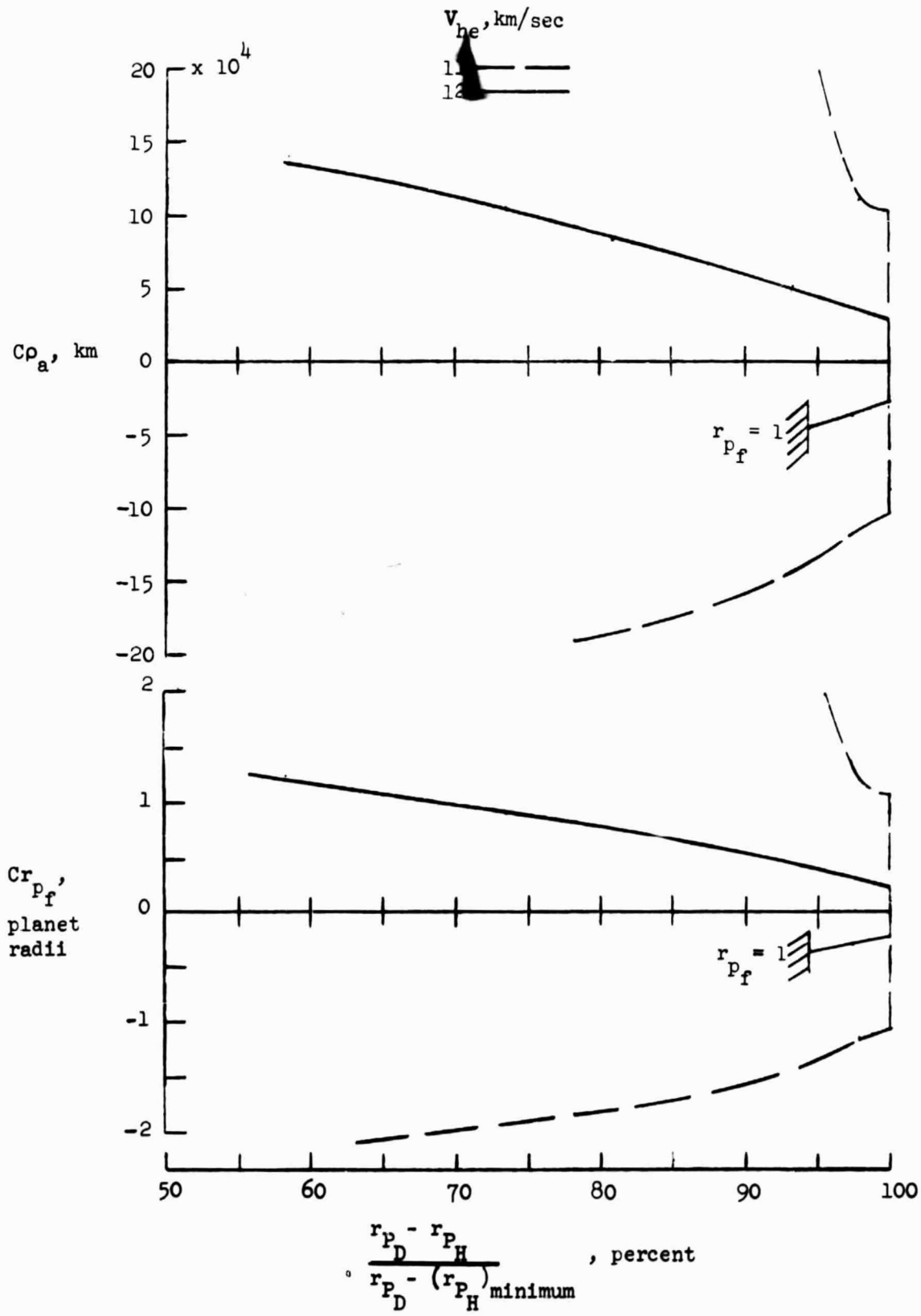

(b) Corridors for flyby distance less than 6 planetary radii (fig. 14).

Figure 21.- Concluded.

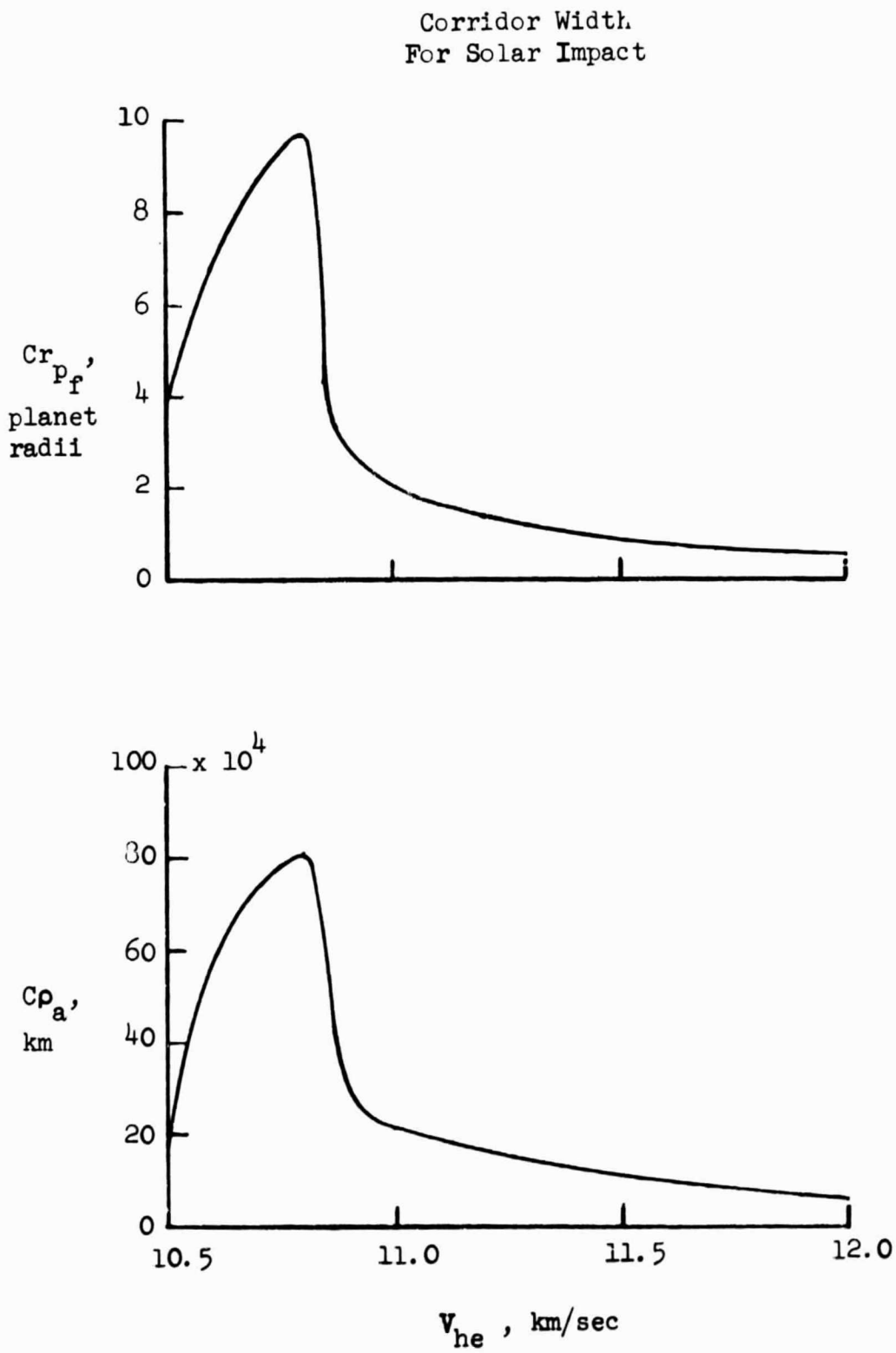

Figure 22.- Variation in Jupiter approach and perigee corridors with launch velocity for flybys which achieve solar impact.

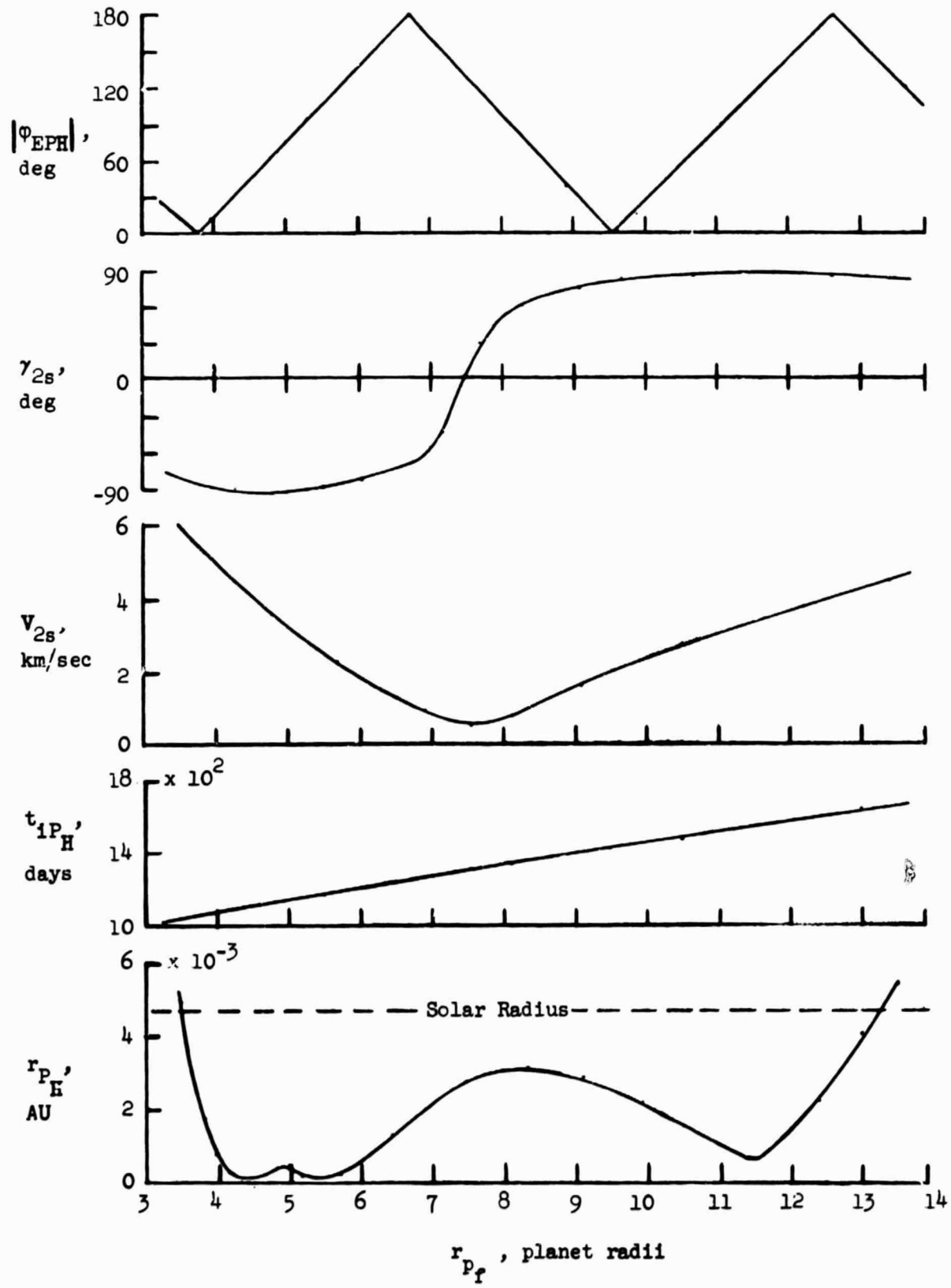

Figure 23.- Variation in flyby parameters with distance of closest approach at Jupiter for the V_{he} = 10.8 km/sec condition yielding maximum encounter corridors (fig. 22).